1 June 1979 • Vol. 204 • No. 4396

$1.50

SCIENCE

AMERICAN ASSOCIATION FOR THE ADVANCEMENT OF SCIENCE

two bright white clouds emerged in the high-velocity jet located at 23°N. These features had eastward velocities of 169 m/sec and circled the planet before dissipating. This was accompanied by an increased drift of 1.5 to 10.0 m/sec, in other features at 15° to 18°N.

The Voyager images show a wedge-shaped turbulent pattern emerging from the southern edge of the North Tropical Zone (NTrZ) and extending equatorward (Fig. 3). Since this pattern is confined in longitude, it is tempting to consider that this feature may be induced by the influence of the GRS. This is not the case, however, since this pattern is observed to drift 0.46°S per day, and in 1977 to 1978 two wedge-shaped systems were present. By August of 1978, one system had dissipated leaving the present pattern with the southern edge of the NTrZ contracted northward to 19° latitude. When this is the case, dark brown clouds similar to those seen in the Voyager data have been present. During periods when the belts near 30° and 35°N are wider, similar low albedo features also appear in this region. Dark brown clouds correspond to enhanced regions of 5-μm emission, indicating a relative absence of high zonal clouds.

Inspection of the equatorial zone of the Voyager data indicates several plumes similar to those reported by Pioneer investigators. At the time of Pioneer 10 and 11, the plumes were well developed and drifting at a rate of 4 to 6 m/sec relative to the mean motion of the dark gray features between the bright areas. Since the beginning of 1975, the velocity of the plumes has slowed to approximately that of the surrounding features; hence, their distinctive character has diminished, making continuous trackings difficult.

This study serves to introduce ground-based data concerning the morphology, origin, longevity, and long-term drift rates of cloud features, and to indicate how this material is being integrated with Voyager data.

RICHARD J. TERRILE
Jet Propulsion Laboratory, California Institute of Technology, Pasadena 91103

RETA F. BEEBE
New Mexico State University, Las Cruces 88003

References and Notes

1. The Target Selection Working Group includes the following participants: R. F. Beebe, G. E. Hunt, A. P. Ingersoll, A. L. Lane, E. Miner, J. Mitchell, T. Owen, J. Pirraglia, B. A. Smith, R. J. Terrile, and R. West.
2. Photographic data were provided by New Mexico State University and Lowell Observatory, and 5-μm imaging was acquired at Palomar and Mauna Kea observatories [see R. J. Terrile *et al.*, *Science* **204**, 1007 (1979)]. Data from the observatory phase of the Voyager Mission were also used in targeting.
3. B. M. Peek, *The Planet Jupiter* (Faber & Faber, London, 1958), presents a historical summary and an explanation of nomenclature. B. A. Smith and G. E. Hunt [in *Jupiter*, T. Gehrels, Ed. (Univ. of Arizona Press, Tuscon, 1976), pp. 568–569] present a summary of zonal velocities.
4. J. W. Fountain, D. L. Coffeen, L. R. Doose, T. Gehrels, W. Swindell, M. G. Tomasko, *Science* **184**, 1279 (1974).
5. R. J. Terrile and J. A. Westphal, *Icarus* **30**, 247 (1977); R. J. Terrile, thesis, California Institute of Technology (1978).
6. E. J. Reese, *Icarus* **17**, 57 (1972).
7. J. A. Westphal, K. Matthews, R. J. Terrile, *Astrophys. J.* **188**, L111 (1974).
8. Catalogued data are available on request from the Astronomy Department, New Mexico State University, as Technical Notes TN-75-50, TB-77-58, TN-78-61, and TN-79-63.
9. We thank A. S. Murrell, C. F. Knuckles, L. A. Youngblood, B. C. Cress, and J. A. Westphal for assistance. Work was supported in part by NASA grant NGL 32-003-001 and NSF grant AST 77-22962. This report presents the results of one phase of research carried out at the Jet Propulsion Laboratory, California Institute of Technology, under contract NAS 7-100, sponsored by NASA.

23 April 1979

The Jupiter System Through the Eyes of Voyager 1

Abstract. *The cameras aboard Voyager 1 have provided a closeup view of the Jupiter system, revealing heretofore unknown characteristics and phenomena associated with the planet's atmosphere and the surfaces of its five major satellites. On Jupiter itself, atmospheric motions—the interaction of cloud systems—display complex vorticity. On its dark side, lightning and auroras are observed. A ring was discovered surrounding Jupiter. The satellite surfaces display dramatic differences including extensive active volcanism on Io, complex tectonism on Ganymede and possibly Europa, and flattened remnants of enormous impact features on Callisto.*

In a flurry of observational activity, Voyager 1 arrived at the planet Jupiter on 5 March 1979. One hundred days earlier, however, the resolution of Voyager cameras (*1*) had already exceeded the best resolution available from ground-based telescopes. About 30 days before encounter, their resolution and image quality were comparable to those of the best Pioneer 10 and 11 images. The effective resolutions at encounter for Jupiter and three of the four Galilean satellites (Io, Ganymede, and Callisto) were only a few kilometers. This improvement in resolution is comparable to the transition from naked-eye observations of Earth's moon to the best ground-based telescopic photographs. Comparable improvements have been achieved in time resolution—that is, in the frequency and regularity with which observations are made.

The approximately 18,000 photographs taken by Voyager 1 in the Jupiter system have led to many new data products and scientific findings, including color motion pictures of the dynamics of the Jovian clouds; images of Jovian lightning and auroras; and the discoveries of a Jupiter ring system, of the elongate shape of Amalthea, of a major system of active volcanoes and substantial recent surface modification of Io, and of novel fracture systems and presumptive tectonic activity on Ganymede and Europa.

The atmospheric dynamics, reducing atmospheres, icy satellites, rings, and other features of the Jovian system give it an environment very different from that of the terrestrial planets with which we have now become familiar. The bodies in the Jupiter system explored by Voyager 1 do not resemble closely either the planets in the inner solar system or one another. The wide range of unexpected findings is due both to the real differences between the outer and the inner solar system and to the depth of our prior ignorance, caused in part by the 4 astronomical units (AU) that separate Earth and Jupiter. The sense of novelty would probably not have been greater had we explored a different solar system. It seems clear that analyses of Voyager 1 data and of data to be acquired by the Voyager 2 and Galileo spacecraft will provide major insights into the origin and evolution of the solar system and, through comparative planetology, of our own planet.

Jupiter: Global atmospheric structure. To obtain the best space-time color coverage of Jupiter's changing atmosphere during Voyager's approach and encounter, several observational strategies were followed (*2*). From 60 to 12 days before encounter (E − 60^d to E − 12^d), multicolor images were taken every 72° of longitude (one-fifth of a Jovian rotation) (*3*). Resolution ranges from 1200 down to 240 km per line pair (lp) for the last systematically scheduled whole-disk mosaics (*4*). Approximately 9300 single-color images were obtained during this period.

From E − 12^d until encounter, Jupiter was too close to be covered by mosaics of reasonable size, and it was necessary to selectively target various patterns of images for specific features. Because of the complexity of the spacecraft com-

0036-8075/79/0601-0951$02.00/0

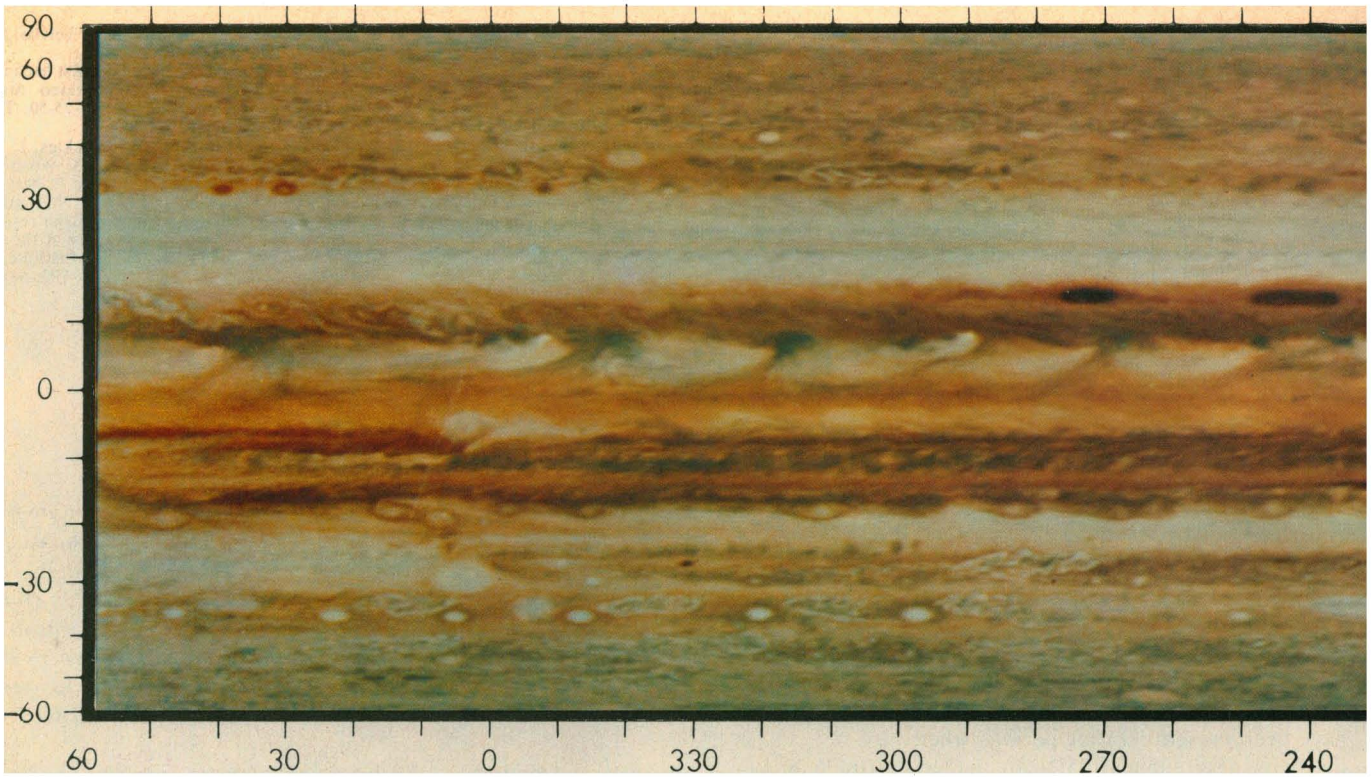

Fig. 1. Cylindrical projection of Jupiter on 1 February 1979. Ten three-color images (orange, green, blue) obtained during a single Jovian rotation at a resolution of 600 km/lp were used to form this mosaic. Longitude is in System III (1965) (*3*), and latitude is planetographic. Nomenclature used in this article is identified along the right margin. This mosaic shows Jupiter on rotation 65, counting from the first Voyager 1 images on 6 January 1979. Encounter (5 March 1979) occurred during rotation 141.

mand sequence, this target selection took place 30 days before execution, thus demanding a 30-day extrapolation of Jovian weather (*5*). The fact that most targets were seen as predicted in spite of longitudinal drift rates ranging from −3° to 10° per day illustrates one of the truly remarkable characteristics of the Jovian atmosphere. From E − 12^d until encounter, about 6000 images were taken, including simultaneous wide-angle images, as the resolution improved from 240 to 6 km/lp. During the month following closest approach, multicolor coverage was continued at a solar phase angle of about 115°, involving some 2200 images. Both the lit crescent and the dark side were photographed during this period, the latter with relatively long exposure times.

To date, we have subjected only a modest fraction of the atmospheric images to quantitative photometric, colorimetric, and dynamic analysis. Yet we have learned much about the Jovian clouds and their motions. The discussion that follows is loosely organized according to the atmospheric belts and zones of Jupiter, which are distributed in latitude. Figure 1 shows the full Jovian cloud surface (>360° of longitude) in a mosaic made by projecting whole-disk images at E − 30^d (cover and Fig. 2) onto a cylindrical grid. We have used the traditional nomenclature of Peek and others (*6*)—North Temperate Zone (NTeZ), North Tropical Zone (NTrZ), North Equatorial Belt (NEB), Great Red Spot (GRS), and so on—with adjustments for the appearance of Jupiter at about the time of Voyager 1 encounter. According to these traditional designations, the zones are bright and white, the belts darker and browner. The Great Red Spot resembles the zones, having anticyclonic vorticity (clockwise in the north, counterclockwise in the south) and low infrared temperatures, the latter suggesting high clouds and upward motion relative to that in the belts (*6-8*). Relative to System III (*3*), the winds are mostly zonal (east-west) with highest velocities at the edges between belts and zones. These cloud bands, the zonal currents, and individual features such as the GRS and white ovals (−38° latitude) are all quasi-permanent features of the atmosphere, with lifetimes of 50 years or more (*6*).

An important goal of the atmospheric investigations was to test this traditional picture by studying Jupiter at high resolution, and in general the picture has proved to be accurate. Velocities were measured by tracking features as small as 200 km over time intervals as short as 2 hours. Because atmospheric wave velocities are strong functions of wavelength, the agreement between velocities measured at widely different scales suggests that mass motion rather than wave propagation was observed. Also, by tracking features in images taken only 2 hours apart, one substantially eliminates errors due to time-dependent morphological evolution of features. The latitudinal variation of velocity appears to be smooth.

The latitudes of eastward currents (E) and westward currents (W) are approximately 50°W, 47°E, 44°W, 41°E, 38°W, 35°E, 30°W, 23°E, 18°W, 8°E, 0°E, −8°E, −16°W, −23°E, −28°W, −32°E, and −35°W (see Fig. 1). Starting at 23° latitude in this sequence, the measured eastward velocities are 150, −20, 120, 90, 130, and −50 m/sec. The equator, although a relative minimum within the equatorial region, nevertheless has an eastward velocity of 90 m/sec. These latitudes and velocities generally confirm the ground-based picture. The association between currents and morphology is also confirmed, with the zones, the GRS, the white ovals, and other bright-centered spots (as at latitudes 31° and −35°) all being anticyclonic. The NTeZ is a major exception, being a region of cyclonic shear with a westward current on its northern edge. The latitudes from 25° to

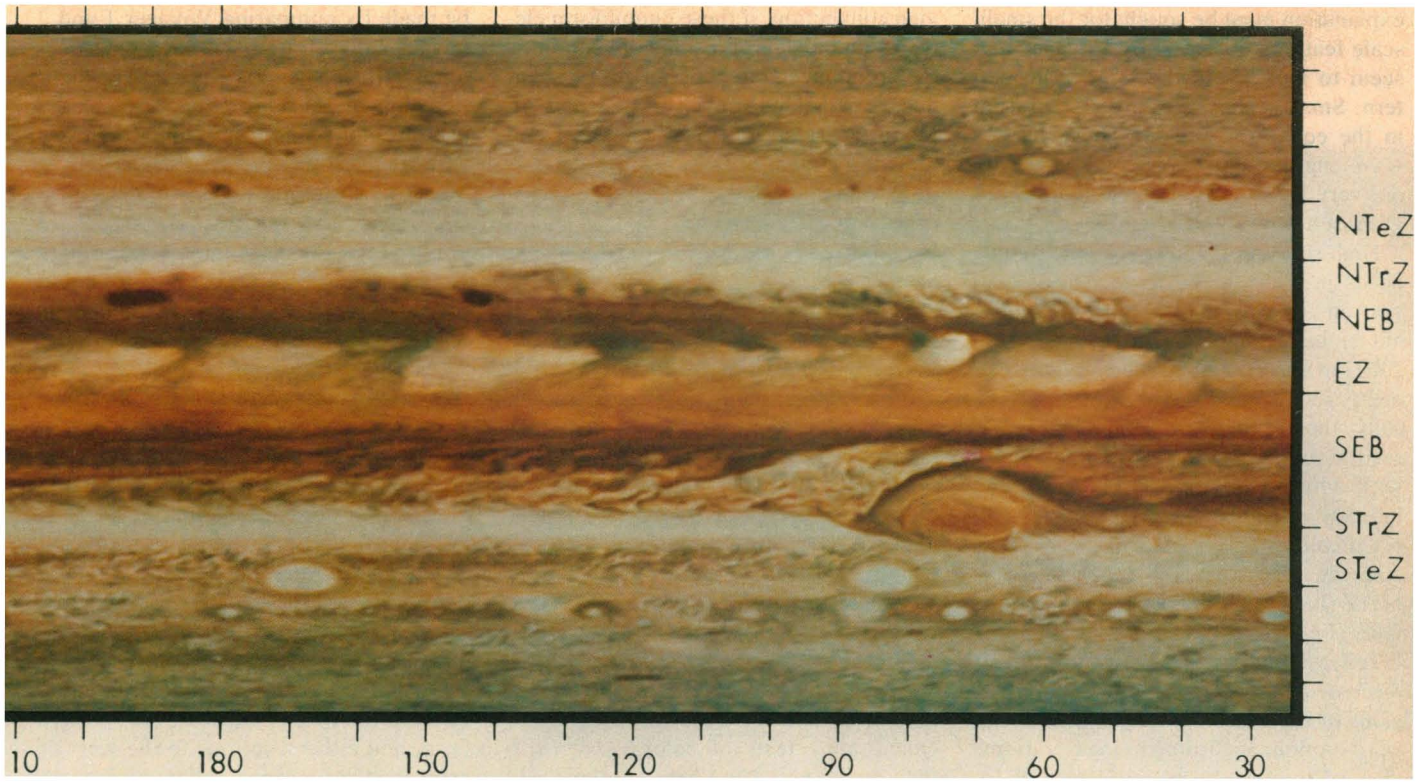

30° are often dark, however, as they were during the 1974 Pioneer encounters (*5*, *9*). Conversely, the latitudes from −25° to −30° changed from light to dark since the Pioneer encounters, although the velocities around both the NTeZ and the STeZ did not change (*10*). Thus the zonal velocity structure may be a more stable feature than color or albedo.

Convection and vertical motion. Another pre-Voyager view, developed largely from Pioneer observations (*9*), was that the white features on the equator are plumes trailing behind (to the west of) small, bright centers of rising motion. Again, Voyager observations, with good space-time coverage, lend support to this view. Rapid brightenings, followed by spreading of the bright cloud material with time constants of 50 to 100 hours, were observed repeatedly in the equatorial region at the plume heads. Figure 2, taken 4 days after the cover image, shows one such bright region. Figure 3 shows a time-lapse sequence of brightenings at the NEB-NTrZ interface, just to the north of the equatorial region (Fig. 1). Such brightenings are also observed at the SEB-STrZ interface to the west of the GRS. Thus, rapid ascent seems to produce white material, suggesting that red material at high altitudes, such as in the GRS, is formed by a different mechanism or originates at different (probably deeper) levels in the atmosphere.

The rapid brightenings tend to be isolated events, especially at the equator, and therefore suggest a triggering mechanism. As seen in Fig. 1, the plumes seem to form a 12- to 15-wave pattern around the planet that moves eastward at 100 to 120 m/sec. Perhaps the passage of the crests of this wave triggers convective activity, as postulated to occur in Earth's tropics (*11*). If the pattern is indeed an eastward-propagating wave, an

Fig. 2. Whole-disk view of Jupiter on 5 February 1979 (rotation 76), 4 days after the view shown on the cover (rotation 65). A bright plume is seen just north of the equator; the satellite Io is seen in transit to the east of the Great Red Spot, and Europa is visible off Jupiter's bright limb. Resolution is 525 km/lp.

explanation must be sought for the small-scale features observed by Voyager that seem to move with the large-scale pattern. Small-scale waves are also present in the equatorial region. These have a wavelength of approximately 600 km, are very localized, and have lifetimes of at most a few Jovian rotations.

High-resolution images of the plume heads provide further evidence of convection and vertical motion (Fig. 4). The nuclei have a horizontal size of about 2000 km and contain individual puffy elements 100 to 200 km in size. Morphologically, these smaller clouds resemble terrestrial cumulus and contrast sharply with diffuse, filamentary features found in many other regions of Jupiter.

Cumuliform elements 100 to 200 km in size are also found in the NTeZ and NTrZ (Fig. 5), as well as in the STrZ and GRS (Fig. 7). With the exception of the NTeZ, which is somewhat anomalous as discussed earlier, these zones are all regions of high-altitude clouds and net upward motion, according to the traditional view of Jupiter. A special feature of Jovian convection, if these cumuliform elements do indeed represent convection, is the pronounced effect of horizontal shear due to zonal currents (Figs. 5 and 6). Features are stretched by the shear and form a diagonal pattern. Two such patterns on either side of an east-west current form a trailing chevron that makes the current visible in both of these Voyager images.

The dark belts, the brown spots, and the equatorial blue-gray regions have been identified from ground-based studies (*8*) as areas of high 5-μm emission, low cloud altitudes, and presumed sinking motion. Conversely, the reddish material within the GRS exhibits all the opposite characteristics (*12*). The Voyager images show new details of all of these features and should allow determination of cloud stratigraphy—for example, the extension of cloud filaments from a white region, partially covering darker clouds. We have imaged several examples of this feature around the borders of the GRS. Quantitative tests of color versus altitude including latitudinal variations will be made by comparing Voyager 1 and 2 images with infrared and photopolarimeter data (*13*). The next steps will be identification of the chromophores and the use of color to infer horizontal velocity versus altitude.

The high-latitude regions have a mottled appearance, superficially suggestive of convection (Fig. 6). However, at high resolution the features tend to resemble the spiral spots at mid-latitudes. Further, the belt-zone pattern of east-west velocity extends to latitudes beyond ±60°, farther than had been recognized before Voyager.

Atmospheric features and their interactions. Dynamically, the GRS is an anticyclonic feature rotating in an anticyclonic shear zone (Fig. 8). The period of rotation within the GRS is about 6 days, suggesting a vorticity of 2.5×10^{-5} sec^{-1} and a Rossby number of 0.2. Typically, small spots approach the GRS from the east, flow around the equatorward boundary, pause at the western cusp, and either continue to the west or enter the GRS peripheral flow. On reaching the eastern cusp, a spot often splits, one part staying with the GRS and the other continuing around to the east (Fig. 8). Alternatively, spots moving westward at the GRS latitude may simply be deflected northward at the eastern cusp, entering the eastward current that flows to the north of the GRS. These cyclonic "circulating currents" are common features associated with mid-latitude features such as the GRS.

Because of its low infrared brightness temperature, the GRS is thought to be a center of rising motion. However, direct evidence of horizontal divergence at cloud-top altitude remains elusive. One large bright feature completed about ten revolutions around the GRS center during the 60 days of Voyager 1 observations without significantly changing its distance from the center (Figs. 7 and 8). The implied upper limit on mean vertical motion is therefore extremely small.

Interactions between spots of equal size (Fig. 9) take place when the poleward member of a pair overtakes the other spot and combines with it. (Both spots are in an anticyclonic shear zone.) The combined mass tumbles for a while, and then usually ejects a streamer to the west and equatorward. The new spot proceeds to the east. Such behavior was not predicted in models published before Voyager (*14*).

Morphologically, the white ovals and other anticyclonic spots at mid-latitudes (Fig. 7) resemble the GRS. All have spiral cloud patterns opening outward into an anticyclonic flow—an S in the north-

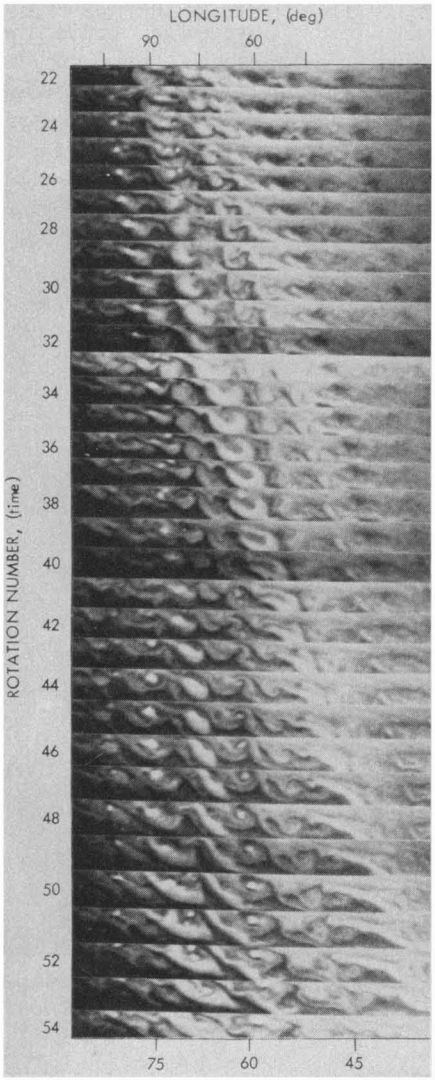

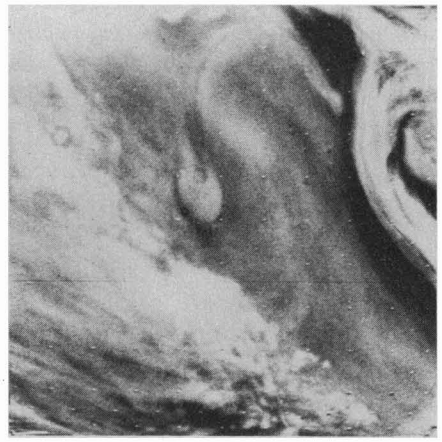

Fig. 3 (left). Time-lapse sequence at latitudes 9° to 16° and longitudes near 60°, showing the disturbed region at the NEB-NTrZ interface. Rotation numbers refer to successive Jovian rotations, as described in the legend to Fig. 1. The individual strips of the sequence were made directly from whole-disk images (such as Fig. 2) and have not been projected to a uniform latitude-longitude system as in Fig. 1. Note also the change in scale as Voyager approached Jupiter. Fig. 4 (above). Plume nucleus (latitude 8°) showing evidence of convective activity. Resolution is 24 km/lp. Distance from top to bottom of the image is 10,000 km. This image was taken through the green filter on rotation 139, 4 March 1979, just 20 hours before Jupiter's closest approach.

Fig. 5 (left). Portions of the NTeZ, NTrZ, and NEB near longitude 190°. North is to the upper left, and the distance from top to bottom is 20,000 km. The puffy clouds of the white NTeZ and NTrZ form a trailing chevron pattern centered on the eastward-moving southern edge of the thin orange band. Such patterns reflect the shear caused by east-west currents. The central brown spot appears "warm" at 5 μm (*5*). It is also seen in Fig. 1 at latitude 14°, longitude 190°. The feature sits in a region of cyclonic (counterclockwise) shear formed by westward and eastward currents to north and south, respectively. Fig. 6 (right). Latitudes 20° to 55°, showing portions of the NTrZ, the NTeZ, and more disturbed regions to the north (north is to the upper left). Note the patterns of puffy clouds, circular spots, and counterrotating vortices in the wakes of other flow features off the picture to the east. The two prominent circular spots, at 32° latitude, are examples of features whose interaction can be studied in Fig. 9. The distance from top to bottom in the figure is 20,000 km. The frame was acquired on 2 March 1979.

ern hemisphere and a reverse S in the southern hemisphere. Many are associated with cyclonic circulating currents to the east and disturbed, cyclonic, wakelike regions to the west (Fig. 7). A difficulty with the "wake" hypothesis, however, is that the individual features in the wake of the GRS move toward it to the east and appear to be blocked by it. An exception to this blocking occurred when bright material crossed the SEB and entered the rapid eastward current in the equatorial zone (Fig. 8).

The disturbed regions include the wakelike regions and also the portion of the NEB-NTrZ interface that is currently at the longitude of the GRS (Fig. 1). There, north-south mixing takes place on scales of thousands of kilometers (Fig. 3). Features are continuously forming and being sheared apart by the zonal currents on either side. The net effect of this intermediate-scale mixing on the large-scale currents has yet to be quantitatively assessed. The existence of these transient disturbances makes the longevity of other features even more puzzling.

Phenomena on the dark side of Jupiter. Phenomena identified so far in the systematic examination of images of the dark (nighttime) hemisphere of Jupiter are diffuse auroras and lightning (Fig. 10). The auroras appear to occur in at least three layers about 700, 1400, and 2300 km above the cloud tops. These diffuse auroral layers are bright by terrestrial standards and vary on time scales of less than 1 minute. They are seen in the north polar region in Fig. 10 but extend equatorward to latitude +60°.

Lightning appears in clusters of bolts and seems to be fairly uniformly distributed over the planet. The strength of individual lightning bolts is comparable to that of terrestrial superbolts observed near terrestrial cloud tops—that is, about 10^{10} joules (*15*).

Jupiter's ring. Jupiter's ring was discovered in a narrow-angle frame targeted halfway between Amalthea and the limb of Jupiter at 16 hours, 52 minutes before closest approach as Voyager 1 crossed the equatorial plane of the Jovian system (Fig. 11, left). This very long exposure (11 minutes, 12 seconds) shows a composition of multiple images of the ring caused by the combined motions of the scan platform relative to the spacecraft, the spacecraft along its trajectory, and a slight rocking of the spacecraft about its center of gravity. Star trails, which look like broken hairpins on this image, establish the directions and durations of these motions when interpreted with the help of engineering data from the spacecraft. Each kink in the star trails corresponds to one image of the ring. (Voyager engineers who contributed significantly to the analysis were C. Hansen, G. Carlisle, T. Duxbury, L. Morabito, and S. Synnott.) This background of stars from the Praesepe cluster was also used to verify that the ring was in the planet's equatorial plane. The ring edge is estimated to be at 1.8 Jupiter radii (R_J) from the center of the planet and thus is well within the Roche limit (2.4 R_J).

The camera had been oriented to record the central region of a possible ring system with the same scale as Saturn's; it was thus entirely fortuitous that it imaged the outer edge of the Jovian rings. However, Acuña and Ness (*16*) had predicted a ring or an undiscovered satellite at 1.83 R_J from an analysis of charged particle data from Pioneer 11, a prediction in remarkably close agreement with this discovery.

At our range of 1.2×10^6 km from the ring, the scale of this picture is ~11 km per picture element, giving an upper limit of ~30 km for the width of the ring. No gradient from the edge toward Jupiter has been detected in the ring brightness. Although accurate radiometric estimates are not available for the ring brightness, the current estimate is 13th magnitude per linear arc-second. The ring was barely visible in two wide-angle frames taken 42 minutes later from a position 0.16° below the Jovian equatorial plane.

Observations of the Jovian satellites. The five regular satellites of Jupiter—Amalthea and the four Galilean satellites (discovered by Galileo in 1610)—were recorded by the Voyager 1 cameras in several colors over a broad range of longitudes, viewing geometries, and resolutions. Basic information on the satellite system is summarized by Stone and Lane (*17*). During the last 2 weeks of approach, complete longitudinal color coverage of the Galilean satellites was acquired at low resolution (20 to 250 km/lp) as they rotated in orbit. Partial longitudinal coverage was also obtained for Amalthea during the last day of approach. Figure 12 shows the best global views of the Galilean satellites acquired during this period. For Io, Ganymede, and Callisto they represent the last views before closest approach, when mosaics were obtained of single hemispheres of these bodies at resolutions of 1 to 7 km/lp. For Europa, the image represents the closest view. The relative color and albedo have been approximately preserved. From ground-based observations it was known that Europa is the brightest (albedo ~ 0.64), Io is also very bright (albedo ~ 0.63) and reddish, Ganymede is intermediate (albedo ~ 0.43), and Callisto is the darkest (albedo ~ 0.17) and least colored (*18*). The images shown in Fig. 12 display the incredible wealth of phenomena on the surfaces of the Galilean satellites: the bizarre color patterns on Io, global-scale linear patterns that traverse Europa, complex interwoven and twisted albedo patterns that lace Ganymede, and enormous concentric systems of multiple bright rings on the crater-riddled surface of Callisto.

Fig. 7. The Great Red Spot and a white oval with its wake of counterrotating vortices. North is at the top, and the distance from top to bottom is about 24,000 km. The first view (top) shows normal color. The second (bottom) shows enhanced color, emphasizing red and blue at the expense of green. Note the puffy features inside the GRS and the reverse-S spirals inside both the GRS and the oval. The large white feature extending over the northern part of the GRS was observed to revolve about the GRS center with a period of 6 days, as seen in Fig. 8.

Close flybys to Io, Ganymede, and Callisto yielded high-resolution images (1 to 4 km/lp) in color and black and white, covering about one-third of the surface of each body. Table 1 and Fig. 13 summarize the nature of the encounters and resultant coverage. The longitudes given are measured west from the mean sub-Jupiter central meridian. Like our moon, the five regular satellites revolve in synchronous rotation about Jupiter, keeping the same face toward Jupiter at all times.

New measurements of the satellite radii are being made by several techniques (*19*). Table 2 presents average values obtained so far; uncertainty estimates incorporate all measurements made for the Voyager images. More precise results are expected as analysis of the data proceeds. The results are in agreement with previous measurements within the quoted errors. Uncertainties in the radii of Europa and Callisto have been reduced considerably. The density of Callisto is closer to that of Ganymede than previous work indicated, and it has been confirmed that Europa has a significantly lower density than Io.

By combining the global coverage and near-encounter data, preliminary base maps of the Galilean satellites have been produced; they are presented in Fig. 14 for reference in the discussion that follows. These airbrush maps portray both albedo and topographic information. More regions will be added from lower-resolution data as image processing is refined and completed.

Amalthea: Shape, color, and albedo. Amalthea, the innermost of the Jovian satellites, was discovered by Barnard in 1892. It is so small and close to Jupiter that it is extremely difficult to observe from Earth.

Ground-based visual and infrared photometry indicated that Amalthea is dark (*20*) and red (*21*), quite unlike any of the Galilean satellites. Voyager 1 acquired a variety of images of Amalthea. A series of navigation frames taken during approach was analyzed by T. Duxbury and S. Synnott to improve knowledge of Amalthea's orbital position, which was needed to target the closest approach sequence. Ten times larger than Phobos and much smaller than the Galilean satellites and terrestrial planets, Amalthea is the first intermediate-size planetary ob-

ject observed in detail. Figure 15 shows three of the best pictures obtained and their observational geometries. These images reveal a small, elongated object (long axis, 265 ± 20 km; polar axis, 140 ± 20 km) in synchronous rotation, keeping its long axis pointed toward Jupiter as expected from Euler dynamical theory. The average geometric albedo is between 0.04 and 0.06, in agreement with ground-based measurements (*20*); several small bright areas have albedos as high as 0.15. These images, with phase angles of 0° to 35°, show Amalthea to have a large phase coefficient (~ 0.04 magnitude per degree), similar to other very dark bodies such as some of the asteroids. The color is very red (0.59 μm:0.41 μm ~ 1.5:1), again in agreement with ground-based UBV (ultraviolet-blue-visual) spectrophotometry (*20*). The brighter spot (Fig. 15, lower right) is, however, gray over this spectral range.

Surface of Io. As can be seen in the global image of Io (Fig. 12) acquired during approach, the surface displays great diversity in color and albedo. In that view, showing the hemisphere facing away from Jupiter, the equatorial region is bright orange-red, mottled by large irregular whitish patches; the polar regions are darker, as was known from ground-based observations (*22*). A host of smaller irregular features, suggestive of albedo and color patterns mixed with topographic forms, are scattered over the surface.

On the basis of this image, it was first thought that the numerous smaller dark spots and the white rings might be impact craters. Closer inspection at higher resolution (Fig. 16) revealed that these pits and markings bear little resemblance to impact craters. The features are irregular in outline and are devoid of raised rims, ejecta blankets, and central peaks. In fact, one of the most striking aspects of Fig. 16 is the complete absence of the classic forms of impact craters over the visible disk. Young, large lunar craters (ages $\leq 10^9$ years; diameters, 50 to 100 km) such as Aristarchus, Copernicus, Kepler, Tycho, and Eratosthenes would certainly be visible at this scale. Even impact craters 5 to 10 km in diameter would be easily detected in Fig. 16, where the resolution is 5 km/lp; none are found. As argued later, the impact crater production rate for the Jovian satellites is probably similar to that for the inner solar system, so that a crater $\geq$ 10 km in diameter would be formed every few million years on the hemisphere visible in Fig. 16 (*23*, *24*). Assuming this rate of cratering, Io is evidently being resurfaced by erosion or deposition, so that craters $\geq$ 10 km in diameter are erased in $\sim 10^7$ years or less. On closer inspection of Io's surface (Fig. 17, b to d) at a resolution of ~1 km/lp, no craters even 1 or 2 km in diameter were found. The age of Io's surface is then, by the same argument, 10^6 years or less. Uncertainties in the actual impact flux for Io could increase these maximum age estimates somewhat, but probably by not more than a factor of 10.

Figure 17 provides direct evidence of at least one process that is renewing the surface of Io: the surface is dominated by volcanic features. More than 100 caldera-like depressions, as much as 200 km across, occur throughout the region photographed (see Fig. 17a). Many show

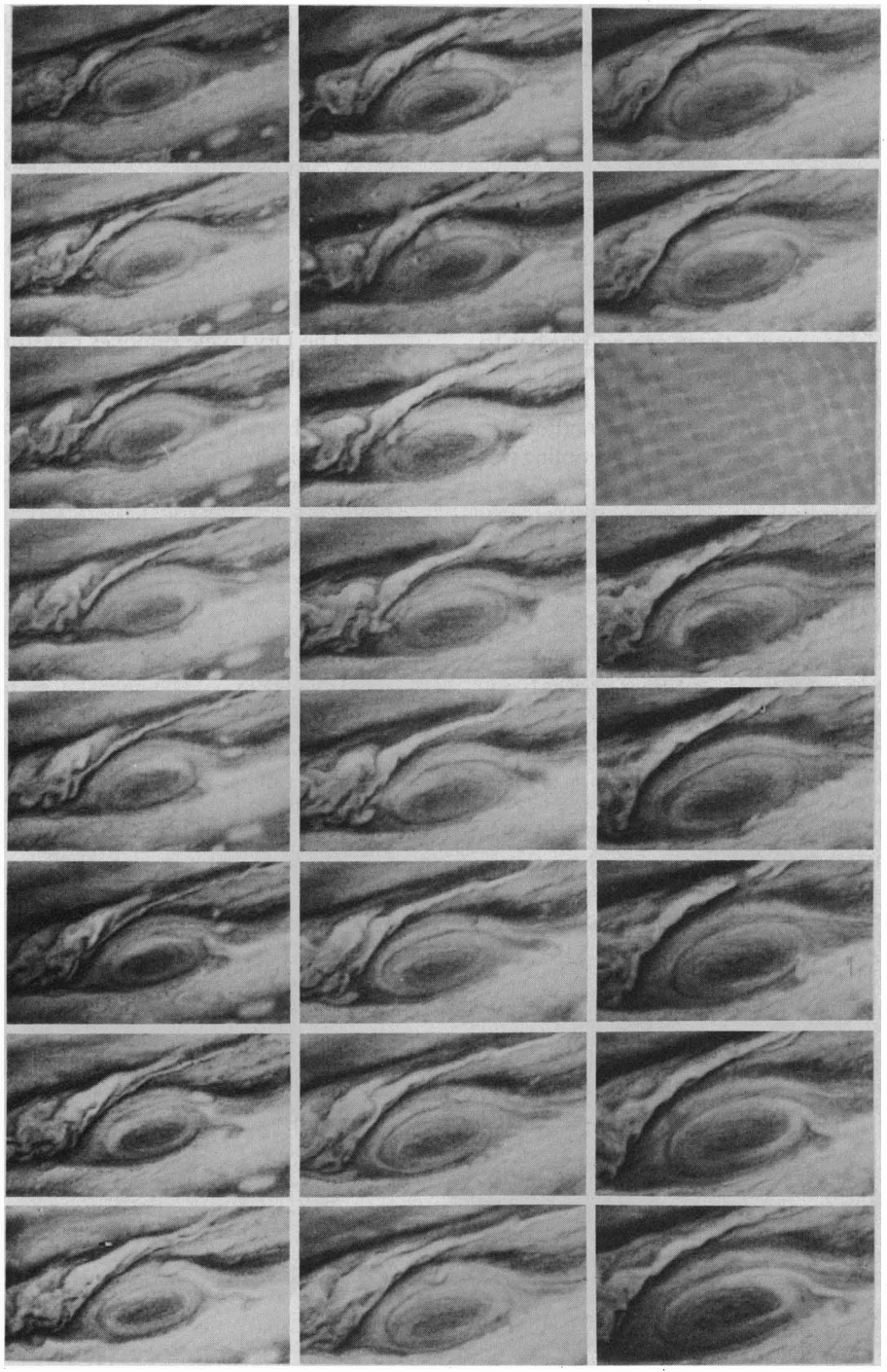

Fig. 8. Time-lapse sequence of flow around the Great Red Spot imaged in blue light. Every odd Jovian rotation is shown, starting with rotation 23 at the upper left, continuing down each column in turn, and ending with rotation 69 at the lower right. Rotation 59 was not imaged because of a spacecraft trajectory maneuver. Follow the two white spots initially in the dark band to the east (right) of the GRS. In the center frames, note also the relatively rare "eruption" of white material across the dark band to the north of the GRS, followed by rapid eastward flow out of the picture. The GRS is approximately 10^4 km wide in its north-south direction.

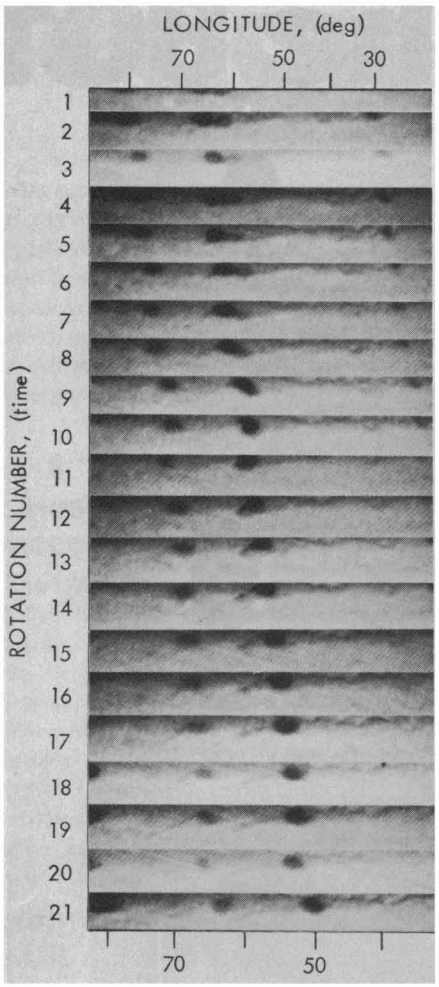

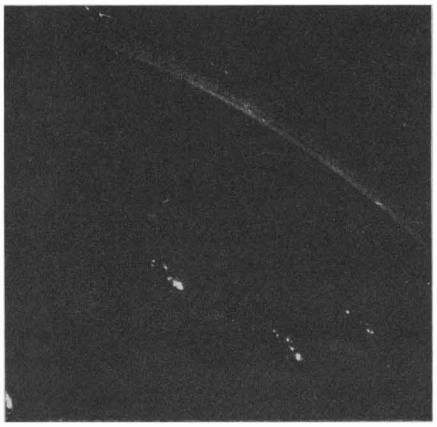

Fig. 9 (left). Time-lapse sequence at latitudes 28° to 34° and longitudes near 60°, showing the interaction of two anticyclonic dark spots. Figure 6 shows similar spots at higher resolution. As explained in the legend to Fig. 3, geometric distortions have not been removed. The two spots, initially at longitudes 62° and 67°, combine to form one spot that ejects a streamer starting on rotation 12. Fig. 10 (right). Dark-side multiple-image view of Jupiter. This wide-angle image was taken 6 hours after closest Jupiter approach while the spacecraft was in eclipse. Jupiter's north pole is on the limb approximately midway along the auroral arc. Several areas of lightning are seen on the disk. Since the scan platform slewed twice during this 3-minute, 12-second exposure, the picture consists essentially of exposures of 35, 35, and 85 seconds, each displaced from the others. The arc of limb is about 30,000 km long.

complex radiating volcanic flows and resemble terrestrial composite collapse calderas (Fig. 17c). Like martian calderas, those on Io are significantly larger than those on Earth; most terrestrial calderas are only a few kilometers in diameter. In contrast to most terrestrial and martian calderas, however, very few on Io appear to be associated with significant topographic volcanic constructs.

The calderas on Io can be divided into two broad classes, those with flows and those without, the latter being more common. The simplest type has no visible flows or albedo markings (Fig. 17a). More commonly, calderas are surrounded by diffuse halos or bright and dark patterns (Fig. 17d). Narrow radial flows varying from black to very complexly colored (reds, yellows, violets, and browns) are associated with about half of the calderas. The flows are large by terrestrial standards, lengths of several hundred kilometers and widths of several tens of kilometers being very common. The patterns, commonly coupled with the absence of discernible relief, suggest low-viscosity flows.

The intervolcanic regions consist of featureless smooth plains occurring at various stratigraphic levels, separated by an assemblage of scarps of unusually uniform relief (Fig. 17, a and b). Topographically, the plains are featureless and smooth. The scarps are probably polygenetic, as they display diverse morphological forms. Some appear to be due to normal faulting (Fig. 17b). Some idea of the topographic relief is provided by measurement of the shadow cast by the pointed mountain on the terminator side of the graben in the upper right of Fig. 17b; the relief here is ~2.1 km. The graben is ~1 km deep; scarps typically are on the order of a few hundred meters high. A few scarps resemble volcanic flow fronts, although most show jagged, irregular, cliff-rimmed edges suggestive of some unknown erosional process causing scarp retreat, perhaps related to volcanic heating. An especially suggestive case, in the central right part of Fig. 17a, shows remnants of the preexisting surface extending southward from an elongate mesa. The general impression gained is that the surface is composed of multiple layers of uniform thickness exposed at a variety of depths.

Isolated mountains with very rugged relief (Fig. 17a, lower right) occur mainly in the polar regions. From pictures of the limb and from shadow measurements

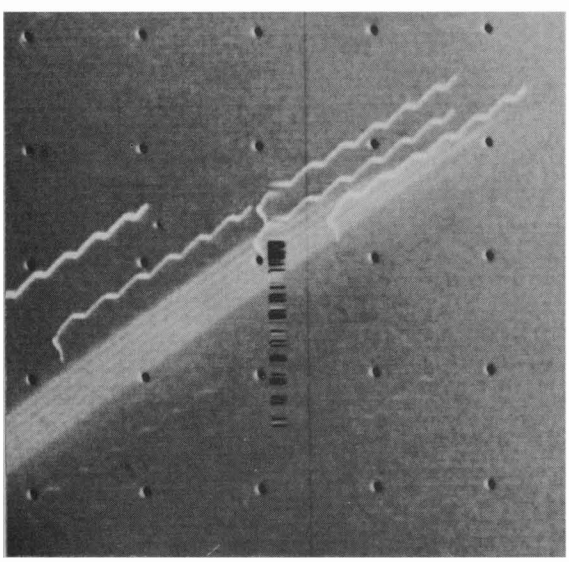

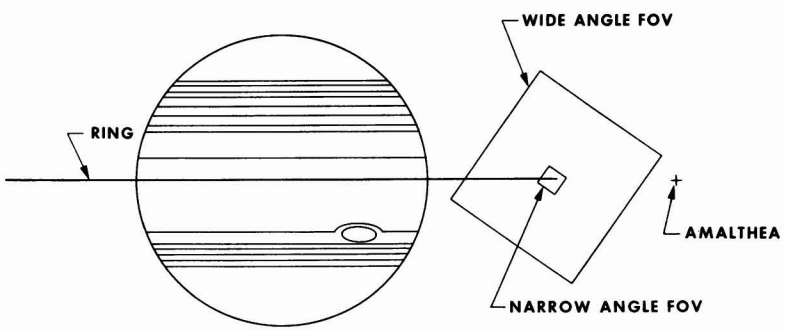

Fig. 11. (Left) Multiple images of Jupiter's ring. Six individual ring images (see text) are shown along with several trailed star images (wavy lines). The dark dots are reseau marks placed on the vidicon faceplate for geometric calibration purposes. The dark vertical lines near center are caused by a data "dropout" as the picture was being received at the tracking station. (Right) Diagram of Jupiter and its ring showing the location of the narrow-angle frame, the wide-angle field of view (*FOV*), and Amalthea. A wide-angle image shuttered simultaneously with the narrow-angle image was saturated by the high-energy particles surrounding Jupiter and therefore does not show the ring.

close to the terminator, it is estimated that typical relief is ~10 km. Some of the rugged mountains are dissected by faults and graben (Fig. 17a). Although they do not resemble volcanic features such as calderas, some of the mountains are surrounded by diffuse halos (Fig. 17), possibly reflecting volcanic eruption from the graben. The general appearance of the rugged surfaces suggests tectonic fracturing and tilting of surface blocks. Perhaps these surfaces are remnants of an older crust.

Active volcanism on Io. Probably the most spectacular discovery of the Voyager mission has been the existence of active volcanoes on Io, erupting materials to heights of several hundred kilometers above the surface. The first discovery of an active volcanic eruption is described by Morabito *et al*. (*25*); it appeared as an enormous umbrella-shaped plume rising 270 km above the bright limb. Since this discovery, six additional volcanic plumes have been found (Table 3); most have been seen several times. In the likely case that the trajectories are ballistic, the altitudes, measured on images taken in the clear filter, imply eruption velocities of several hundred meters to ~1 km/sec. Figure 18 shows a variety of important aspects of the plumes. Plume 3 is very symmetrical (Fig. 18c) and erupts from a white-ringed vent (Fig. 18a and center of Io image, Fig. 12). When seen against the disk the plume is dark (Fig. 18b), implying low albedo for the erupting material. By contrast, plume 2 (Fig. 18, d to f) is irregular,

Fig. 12. Global color images of the four Galilean satellites. The subspacecraft longitude and resolution for the images are: Io (~140°, 16 km/lp), Europa (~300°, 36 km/lp), Ganymede (~320°, 47 km/lp), Callisto (~350°, 22 km/lp). The satellites are shown to scale; Io is slightly larger than the moon, Ganymede larger than Mercury. Relative albedo and color are also qualitatively preserved, although colors may be somewhat exaggerated by the processing and the full range of albedo (over a factor of 3 between Europa and Callisto) cannot be easily displayed.

Table 1. Summary of satellite close approaches.

Satellite	Subspacecraft		Range (km)	Best resolution (km/lp)	Phase angle
	Latitude	West longitude			
Amalthea (JV)	−5°	298°	417,100	7.8	28°
Io (JI)	−80°	340°	20,500	1*	81°
Europa (JII)	−0.2°	338°	733,800	33†	2°
Ganymede (JIII)	+24°	277°	114,600	2	119°
Callisto (JIV)	+82°	320° to 283°	126,100	2.3	92°

*Best Io resolution was limited by image smear, not distance of closest approach. †Final Europa images were obtained at a range of 1.8×10^6 km, well before closest Europa approach.

jetting material northwestward, and diffuse in form. The dark material is neutral to green in color (Fig. 18e). In the ultraviolet ratio image (Fig. 18f) this plume shows two components; the central core, seen in visible light, is encased in a much larger, fainter envelope of material that scatters preferentially in the ultraviolet. The ultraviolet component seems to be too bright for a Rayleigh scattering gas; it is more likely due to extremely fine particles or possible resonance scattering by gas.

What causes such violent volcanic activity? To keep a body the size of Io in a state of continuous volcanic activity through geologic time by radiogenic heating would require an unreasonably large fraction of long-lived radionuclides. A model for tidal heating of Io published by Peale *et al.* (*26*) just before encounter seems to be the likely explanation. In this model, Europa and Ganymede induce a forced eccentricity in Io's orbit. This motion causes variations in the amplitude of the large fixed tides produced by synchronous rotation about Jupiter. In this model, no extraordinary amount of radionuclides is required; the heat source will last indefinitely.

Studies of Io's spectral reflectance suggest that the spectra of sulfur-rich materials are good matches for the extremely steep decrease in Io's blue and ultraviolet reflectance (*27, 28*). Also, unlike the other satellites, Io has no water absorption features. Discovery of singly (*29*) and doubly (*30*) ionized sulfur emission in the vicinity of Io's orbit further strengthens the idea that the satellite may be a source of sulfur. It seems likely that sulfur plays a major role in controlling the variations in color on the surface. Sulfur is a very complex substance, occurring in numerous vividly colored (reds, yellows, black, browns, and so on) allotropic forms which have strikingly different properties and optical absorption coefficients that vary with temperature (*28, 31*).

The velocities required to explain the observed heights of the eruption plumes can be achieved by gas expanding along the volcanic conduits from depths as shallow as a few kilometers. The gas may consist predominantly of sulfur or sulfur compounds (such as H_2S and SO_2). On reaching the surface, the gas may become so cold that some fraction condenses into fine particles.

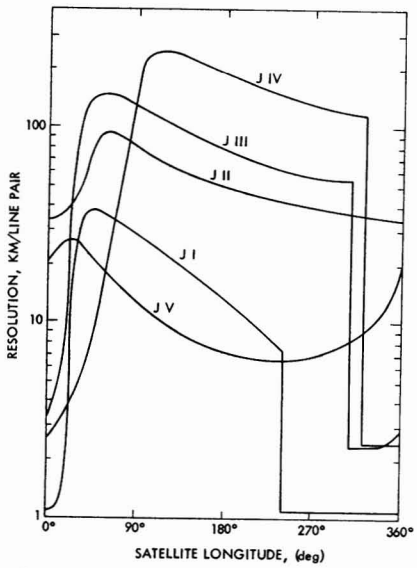

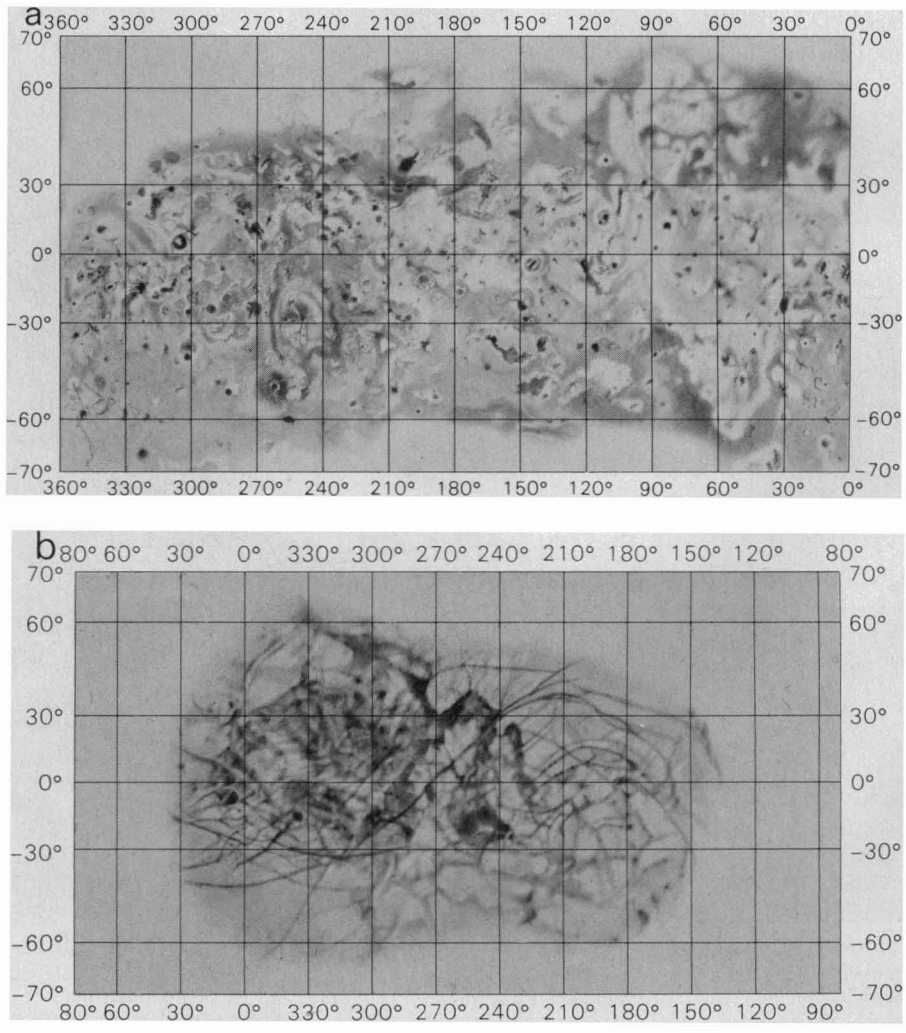

Fig. 13. Resolution versus satellite longitude coverage for Voyager 1. Each of the five largest Jovian satellites (Io, JI; Europa, JII; Ganymede, JIII; Callisto, JIV; and Amalthea, JV) was photographed throughout its final orbit prior to Voyager 1's closest approach. For each satellite, image resolution varies as a function of surface longitude due to the decreasing spacecraft-satellite range during the satellite's orbital period. Consequently, the poorest resolution on the outer moon, Callisto, is substantially worse than the poorest Amalthea coverage. Sharp discontinuities in resolution correspond to the terminator longitudes at the times of closest satellite approach. Because Voyager 1's closest approaches to Io and Callisto were at high latitudes, longitudinal coverage is not completely representative.

Global appearance of Europa. The Voyager 1 trajectory did not include a close approach to Europa. The best resolution achieved was 33 km/lp (Fig. 12). At this resolution, Europa appears distinctly different from the other Galilean satellites. Its surface displays no obvious basin structures and only a few features suggestive of large impacts. In contrast to Ganymede and Callisto, rays from impact craters are notably absent. On a global scale, Europa is characterized by

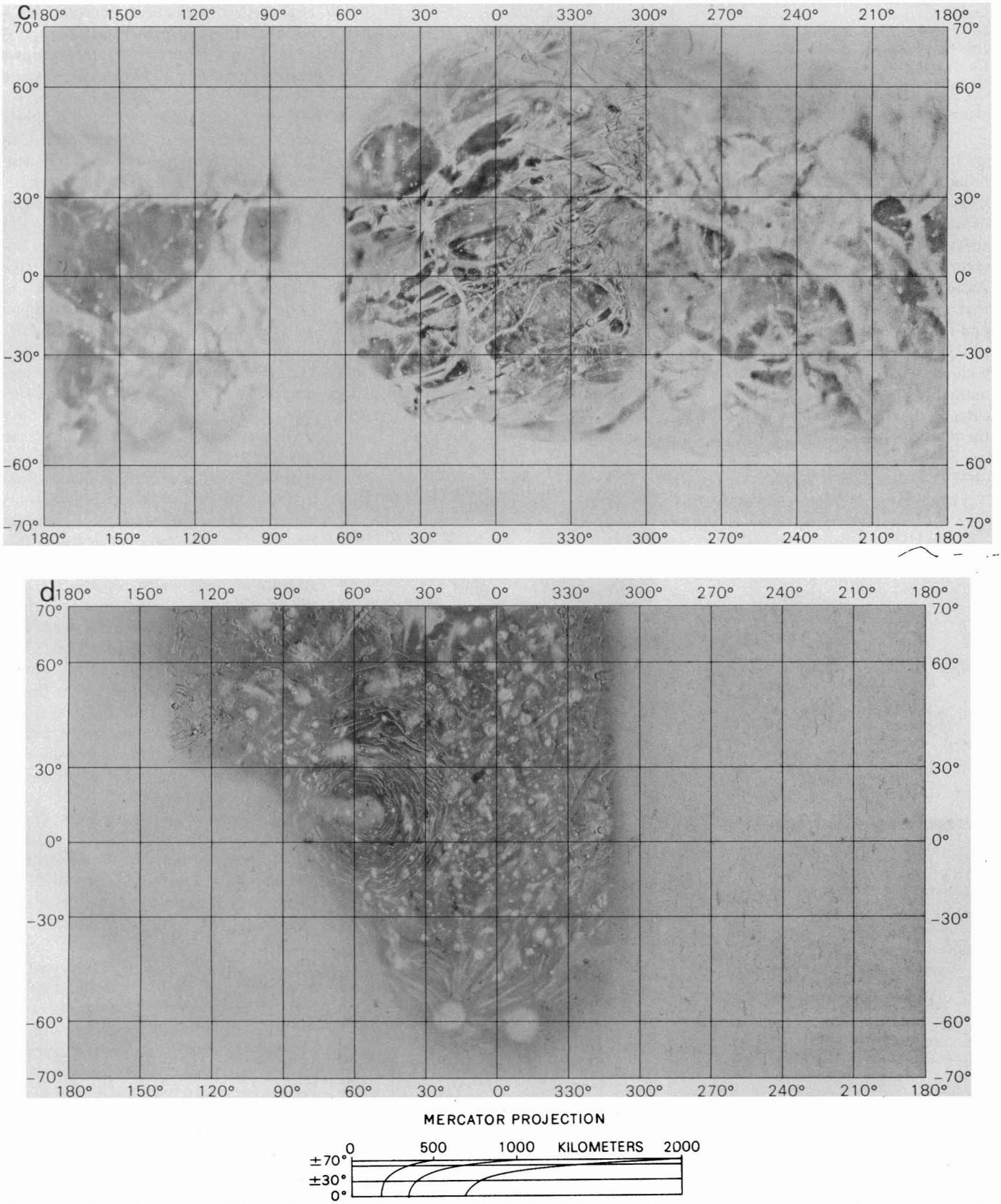

Fig. 14. Shaded relief maps of (a) Io, (b) Europa, (c) Ganymede, and (d) Callisto. These maps have been prepared from images covering a wide range of resolutions: encounter images and high-resolution images from near encounter. They are preliminary and are provided for orientation in the discussions that follow. The scale is 1:100,000,000 (1 cm = 1000 km); both topography and albedo are portrayed. The maps were produced by P. Bridges (Io and Callisto) and J. Inge (Europa and Ganymede) under the direction of R. Batson, all of the U.S. Geological Survey.

Table 2. Satellite diameters and densities.

Satellite	Diameter (km)			Bulk density* (g/cm³)
	Earth-based measurements (*39*)	Pioneer 10 and 11 measurements (*40*)	Early Voyager measurements	
Io	3640 ± 20	3680 ± 60	3640 ± 30	3.53
Europa	3000 ± 200	3104 ± 40	3130 ± 30	3.03
Ganymede	5270 ± 50	5300 ± 50	5280 ± 30	1.93
Callisto	5000 ± 150	4840 ± 40	4840 ± 30	1.79

*Masses assumed are from Anderson *et al.* (*41*). Densities are based on Voyager diameters.

broad, low-contrast, regional albedo markings; the poles are slightly brighter, as was suggested from ground-based observations (*22*). The most striking characteristic visible in Fig. 12 is a pattern of enormous intersecting linear features that are 50 to 200 km wide; some are several thousands of kilometers long. Their distribution is more clearly seen in the pictorial map in Fig. 14. Some of the more prominent features, such as that running diagonally across the center of the map, approximately follow great circles aligned at 45° to one another. Others, principally near longitude 200°W, approximate small circles. These patterns are strongly suggestive of global-scale tectonic processes, induced either externally (as by tidal despinning) or internally (as by convection). The model proposed for Io (*26*) also predicts tidal heating for Europa although about an order of magnitude less. Thus it is possible that Europa is also internally active; its global fracture-like patterns may reflect continuing endogenic evolution.

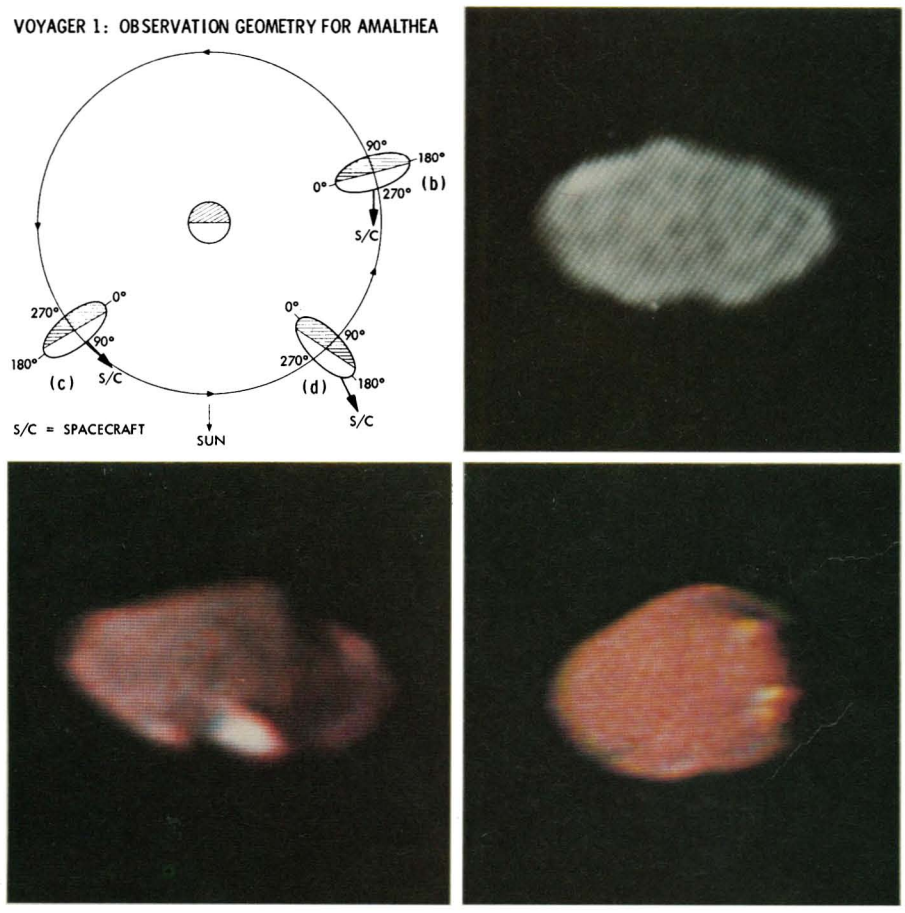

Fig. 15. Amalthea. (Top left) Schematic illustration of the observing geometry for the three Amalthea images shown. The diagram is a view from the north pole of Jupiter; arrows indicate directions of the spacecraft and the sun; the shaded area represents the nightside of Amalthea. (Top right) Subspacecraft longitude, 287°; phase angle, 0°; range, 1,250,000 km; resolution, 25 km/lp. (Bottom left) Subspacecraft longitude, 93.7°; phase angle, 35.5°; range, 694,900 km; resolution, 13 km/lp. (Bottom right) Subspacecraft longitude, 195°; phase angle, 28.6°; range, 425,167 km; resolution, 8 km/lp.

Ground-based near-infrared spectra of Europa indicate large amounts of exposed water, probably in the form of ice (*32*). The revised density (Table 2) of Europa (3.0 g/cm³) relative to Io (3.5 g/cm³) is consistent with the conclusion that a large fraction (20 percent) of Europa is water (*33*). A water and water-ice outer shell as much as 100 km thick is quite possible.

Ganymede. Ganymede is Jupiter's largest satellite and, together with Callisto, represents a class of large, low-density planetary objects that has never before been studied in detail. Its density of 1.9 g/cm³ suggests a bulk composition of ~50 percent water by weight. Evolutionary models of the internal structure have suggested differentiation into silicate-rich core, an ice crust, and either a liquid water mantle (*34*) or a solid, warm-convecting ice mantle (*35*). Ganymede's high albedo and infrared spectrum suggest that water ice is exposed on its surface.

On a global scale (Fig. 12), Ganymede has a variegated surface that superficially resembles that of Earth's moon. Randomly distributed diffuse bright spots suggest the presence of rayed impact craters. The most interesting feature visible in Fig. 12 is the complex of stripes of roughly uniform width, slightly brighter than the average surface, that crisscross the disk in linear, curved, irregular, segmented, and branching patterns. The stripes do not resemble rays from impact craters. They are most apparent in the southwestern part of the disk shown in Fig. 12. The complex intersecting nature of the stripes in this image originally suggested that they might be reflections of tectonic processes.

Higher-resolution images (Figs. 19 and 20) show that the dark background and brighter stripes consist of two distinct terrain types—cratered and grooved, respectively. Cratered terrain contains abundant, predominantly shallow craters ranging from a few to > 50 km in diameter. Grooved terrain is characterized by a complex of closely spaced, shallow grooves that form interwoven networks running parallel to the boundaries of the stripes. The stripes divide the cratered terrain into isolated polygons several hundred to about 1000 km across.

Figure 20b shows that the dark cratered terrain is nearly saturated with craters a few tens of kilometers in diameter. The density of craters of this size is similar to that found in ancient highland cratered terrains on bodies in the inner solar system. On Earth's moon, the ancient cratered terrain is known to date back to

Fig. 16. Computer-generated mosaic of Io made from four sets of images. The diameter of Io is about 3640 km. Resolution in this image is about 8 km/lp, and the center of the image is at latitude −10°, longitude 260°.

a period of heavy bombardment ending about 4 billion years ago. Ganymede's dark cratered terrains probably date back to that same early period. If the cratered terrains were the same age as the lunar maria (~3 to 3½ billion years), which are less cratered by a factor of 10 to 100, then the average impact rate for Ganymede would have to be a factor of 10 to 100 greater than that for the moon during the last 3 billion years. As discussed later, similar cratering rates for Ganymede and the moon are more likely.

Figure 21 shows that the crater density on Ganymede's grooved terrain varies from place to place but is, on the average, about one-tenth that on the cratered terrain. Therefore, the grooved terrain is younger than the cratered terrain and developed over some period of time. Even the youngest sections of the grooved terrain are as densely cratered as the oldest lunar maria and the oldest martian plains units. Formation of the grooved terrain may have ceased several billion years ago, at about the time of extrusion of the oldest lunar mare basalts.

Most of the grooved terrain is a mosaic of discrete systems of grooves, with the grooves of one system ending abruptly at the boundary of an adjacent system. In some places one system transects another. Where the grooved terrain meets the older cratered terrain, the grooves are parallel to the lines of contact. Each system contains a few to several tens of grooves. Systems are ~10 to ~100 km wide and range from ~10 to ~1000 km in length. Individual grooves are a few hundred meters deep, as determined by measurement of shadows near the terminator, and ~5 to ~15 km wide. They are generally arcuate in plan and some have sharp bends; therefore the grooves and intervening ridges cannot have been produced by strike-slip displacement of the crust.

Also, where one groove system transects another, grooves of the older system do not appear to be laterally displaced along grooves of the younger. One example of apparent right-lateral offset of a stripe of grooved terrain can be seen in the center of Fig. 20, however, where a north-south stripe is offset about 50 km. The grooves themselves may have resulted from normal or reverse faulting or from subsurface intrusion of dike systems, causing surface expansion. Local truncation of the grooves at boundaries of other groove systems does, however, suggest possible lateral crustal motion. The fanlike patterns in Fig. 20, b and c, might have been produced by rotation of pieces of the crust that truncate grooves on transverse faults.

A striking fact about Ganymede is the absence of major relief. There are no large basins or large-scale mountainous landforms. Local relief on the bright limb

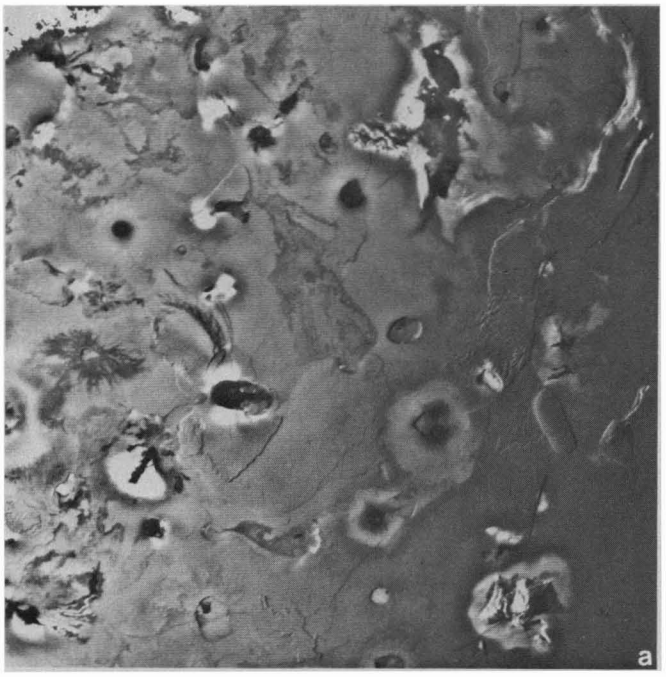

Fig. 17. Imaging of Io. (a) Wide-angle image, centered near latitude −72°, longitude 326° (~1760 km in width, resolution ~4.4 km/lp), showing a variety of volcanic calderas, albedo patterns, vast smooth plains, complex scarps, and rugged isolated mountains. (b) Image centered near −68°, 272° (~450 km in width, resolution 1 km/lp), showing complex graben and irregular scarps near the terminator. (c) Large flow pattern radiating from the central caldera shown in image centered near −53°, 330° (~225 km in width, resolution ~1 km /lp). (d) Complex albedo patterns highlighting the flows, calderas, and volcanic features shown in image centered near −10°, 295° (~600 km in width, resolution ~1.6 km/lp).

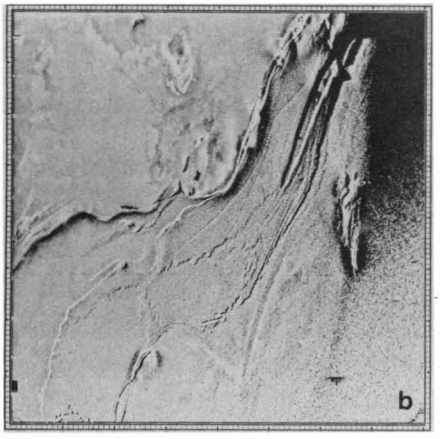

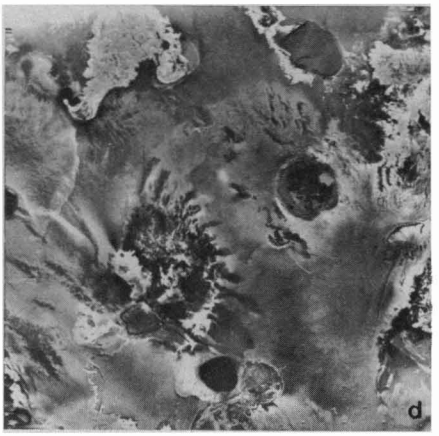

is nowhere greater than about 1 km. This low relief may be the consequence of creep in an icy crust (*36*). Craters of nearly all observed size ranges have a wide range of shapes from moderately deep to extremely shallow (Fig. 20c). Shallow craters in the size range ~10 to ~50 km generally have sharp rims and convex floors, a form rarely observed on the terrestrial planets. Such forms could also be produced by gradual collapse of topography under cold flow.

In summary, the preliminary data suggest that Ganymede had a mobile active crust early in its history, when sections of the older cratered terrain were replaced by grooved terrain. Relief of both large- and moderate-sized topographic forms (basins and craters) probably has been reduced by viscous flow.

Callisto. Callisto, only slightly smaller than Ganymede, has the lowest density of the Galilean satellites, implying that it has large amounts of water in its bulk composition. Its surface is darker than that of the other Galilean satellites, although it has nearly twice the moon's mean albedo. Infrared reflectance spectra show H_2O absorption features; they are weaker than those on Ganymede and Europa (*37*). The Voyager 1 images of Callisto show it to be the mostly heavily cratered object in the Galilean system (Figs. 22 and 23). Like the cratered terrain on Ganymede, the surface of Callisto probably dates back to the period of heavy bombardment ending about 4 billion years ago (Fig. 21). Aside

Table 3. Io volcanic plume inventory.

Plume	Latitude	Longitude	Approximate height* (km)	Remarks
1	−28°	248°	270	Symmetric, first discovered
2	10°	300°	100	Asymmetric, diffuse
3	−5°	145°	100	Symmetric
4	20°	168°	100	Asymmetric, diffuse
5	27°	97°	100	Diffuse
6	16°	109°	100	Symmetric
7	−33°	212°	100	Diffuse

*Heights are measured in visible light. In ultraviolet, images show a larger faint envelope rising to about twice this height.

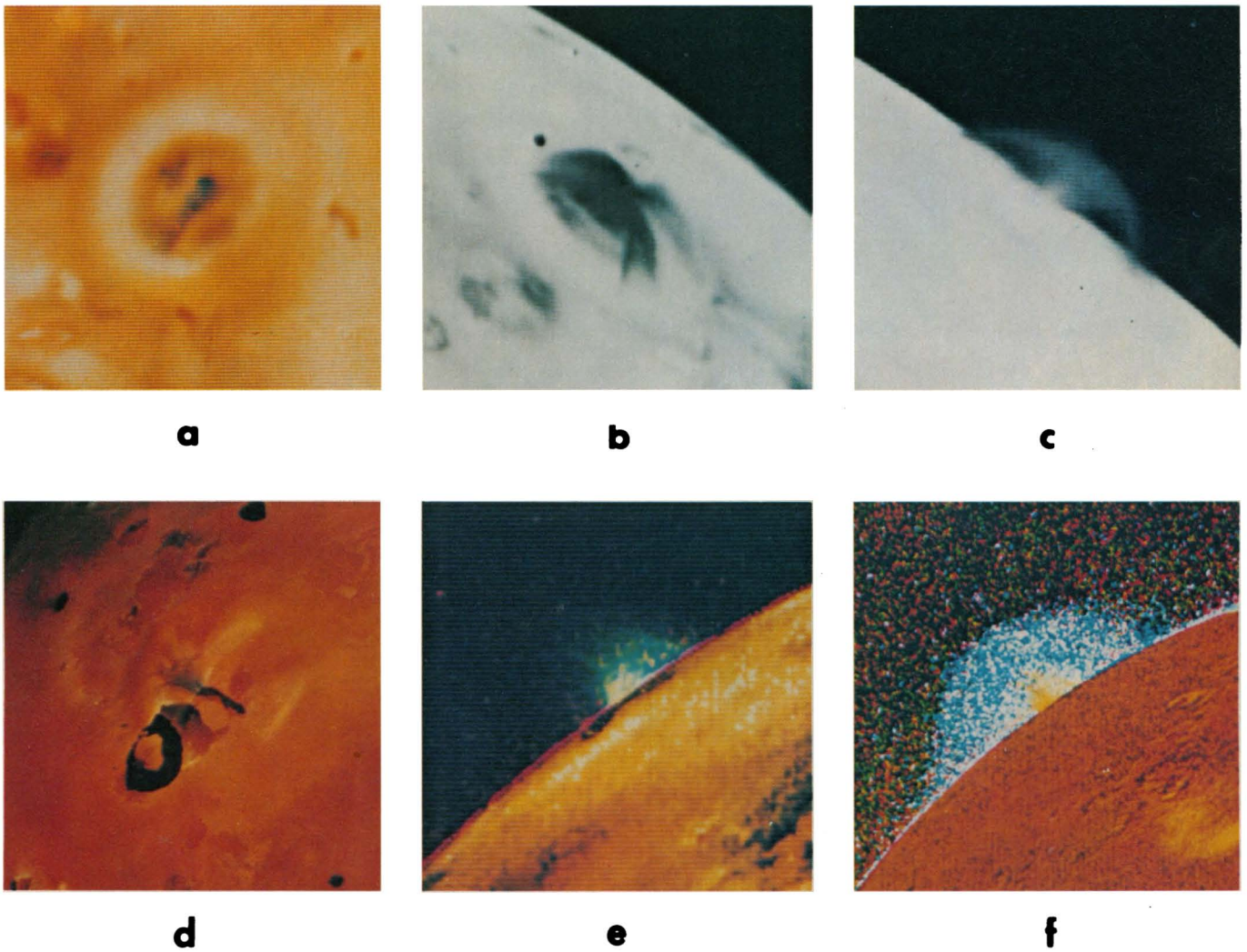

Fig. 18. Views of two active plumes on Io. (a to c) Images of the vent area (a) and eruptions over the disk (b) and bright limb (c) of plume 3 (Table 3), which erupts from the bright ringed area centered in Fig. 12. (d to f) Images showing the vent area (d) and two color-processed versions of the same image set of plume 2 (Table 3) erupting over the limb. The first (e) is constructed from three visible filter images (violet, green, and orange) and shows the core of the plume is greenish relative to Io's surface. The second (f) is a ratio composite in which ultraviolet, violet, and orange images have been divided by green and used as blue, green, and red in the composite. It shows a second component, visible in ultraviolet light, extending far above the central core seen in visible light (e).

Fig. 19. Color image of Ganymede. The image is about 1600 km across, is centered at about latitude 35°, longitude 345°, and has a resolution of about 4 km/lp. Dark cratered terrain, lighter grooved terrain, and many examples of bright ray craters are shown.

from the high crater density, the most striking feature on the hemisphere observed on closest approach is a large multi-ring structure (Figs. 22 and 23). This complicated feature is similar in some respects to large circular impact basins that dominate the surface of the moon and Mercury. The inner parts of these basins are generally surrounded by radially lineated ejecta and several concentric mountainous ring structures that are thought to have formed during the impact event (*38*).

There are some important differences between the large multi-ring structure on Callisto and the multi-ring basins on the moon and Mercury, the main one being the absence of the central basin. The structure consists of a central, bright circular patch about 300 km in diameter surrounded by at least eight to ten bright discontinuous ridges more or less equally spaced, extending out about 1500 km from the center. No radially lineated ejecta can be seen and there are no ring mountains. The flatness and unusual ring spacing are presumably due to the difference in material properties between an ice-rich crust and the silicate crusts of the moon and Mercury. Viscous flow during or subsequent to the impact event probably reduced the topographic relief, leaving a broad albedo feature to record the former presence of the basin.

Crater densities in the smaller size range over most of this hemisphere of Callisto are near saturation. However, the central region of the large basin is far less heavily cratered; crater density increases from the center to the outer

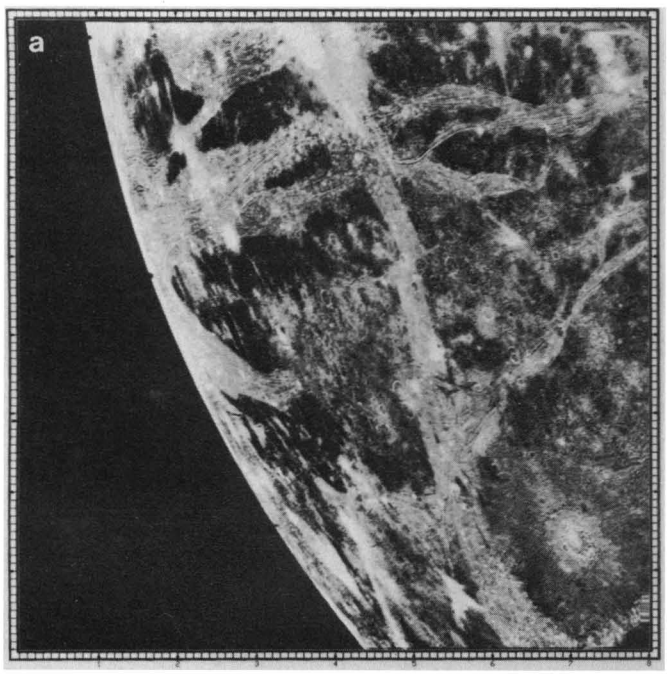

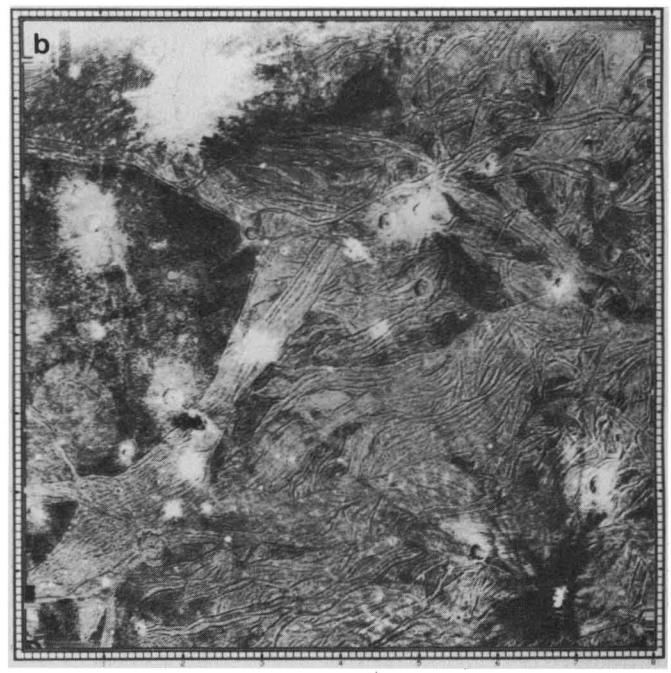

rings, where it reaches the average density of the surface of the satellite. Figure 23, a sketch map of the basin region, illustrates this gradient. These relationships imply that the multi-ring structure was formed relatively late in the period of heavy cratering.

Other large bright circular features are seen near the south limb (Fig. 12). Also, part of another multi-ring structure is visible in a terminator image (Fig. 24). Large impact structures appear to be fairly common on Callisto's surface. One centered near −60° latitude, 20° longitude has some radial features. None of these structures has large topographic relief.

The absence of recognizable large impact structures on Ganymede and the absence of grooved terrain on Callisto suggest basic differences in crustal evolution between these two satellites. The current estimate for the radius of Callisto (see Table 2) suggests a density difference, but not as large as previously thought. Some factors other than differences in the silicate-to-ice ratio, which determines radioactive heating, may be required to account for the differences in surface processes and history recorded on the surfaces of Ganymede and Callisto. Possible factors may be small differences in tidal dissipation or initial accretional heating.

Impact craters: Implications for time scales. The surfaces of the Galilean satellites have a large range of crater densities as well as crater morphologies. The remarkable absence of recognizable impact craters on Io implies either that the flux of impacting bodies is extremely low or that Io's surface is extremely young. The latter interpretation is supported by the discovery on Ganymede and Callisto of densely cratered terrain and the presence of fresh as well as degraded crater forms.

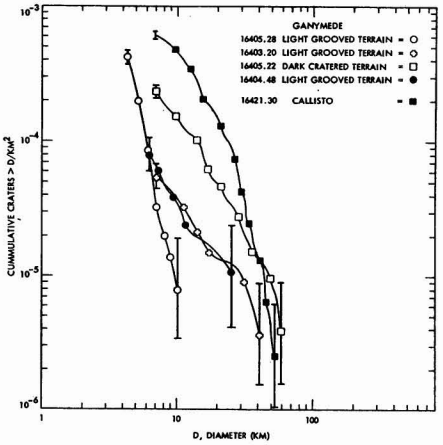

Fig. 21. Cumulative frequency per unit area of craters larger than a given diameter. Shown are curves for heavily cratered Callisto, three samples of Ganymede grooved terrain, and Ganymede cratered terrain.

Studies of the history of cratering in the inner solar system, based on observations of crater populations on younger surfaces and models of cratering rates expected from cometary and asteroidal impacts, suggest that the average crater production rates over the last few billion years were the same on Mercury, the moon, and Mars within a factor of ~2 (*23*). Most young impact craters on the Galilean satellites probably were formed by Mars-crossing asteroids that had been deflected into Jupiter-crossing orbits by close encounters with Mars. Active comets and Earth-crossing asteroids together may account for about 10 to 20 percent of the present flux of impacting bodies. The cratering rates estimated by applying these models to Ganymede and Callisto are roughly similar to the present cratering rate on the moon. The estimated cratering rate on Io is several times higher because of the greater effect of Jupiter's gravity. These are model-dependent rates based on estimates of the populations of planet-crossing asteroids and comets. If other classes of objects were involved the rates might be higher, but they could not be substantially higher without affecting the relatively uniform rate in the inner solar system. Hence, the high density of craters several tens of kilometers in diameter on Callisto and on the cratered terrain on Ganymede was probably produced during late stages of heavy bombardment ~4 billion years ago. Even the grooved terrain, with its much lower crater density, was probably formed close to the end of the period of heavy bombardment. Crater densities in the centers of the multi-ring structures on Callisto are also high enough to suggest that these structures were formed in the early heavy bombardment period ~4 billion years ago.

Craters on Ganymede and Callisto show an extreme range in the preservation of the albedo patterns of rays, suggesting that formation of their craters occurred throughout geologic time. Some process or combination of processes, such as micrometeorite impact, surface gardening, recrystallization, radiation darkening, or simple contamination of the surface by meteorite debris, is causing the rays to disappear with time.

Voyager 2 opportunities. The upcoming Voyager 2 Jupiter encounter (9 July 1979) promises to complement in several significant ways the imaging data returned by Voyager 1:

1) Voyager 1 obtained periodic global images of Jupiter over 3 months. Voyager 2 will extend this time base to nearly 7 months, enhancing observations of the gradual evolution of atmospheric circulation patterns.

2) Voyager 2 will obtain Europa images at a resolution of about 4 km/lp, as opposed to Voyager 1's limit of 33 km/lp.

3) High-resolution coverage (1 to 4 km/lp) will be obtained of the hemispheres of Ganymede and Callisto that were not observed during near encounter by Voyager 1.

4) In response to discoveries made by

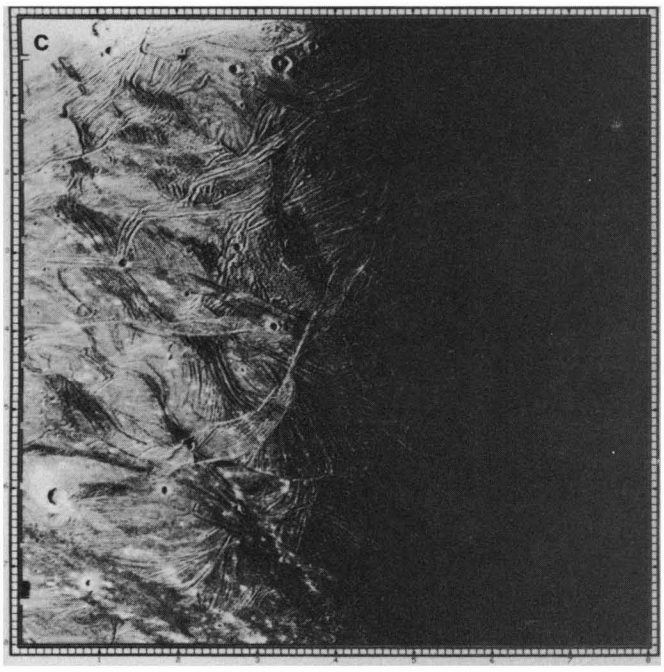

Fig. 20. Ganymede images, showing (a) broad north-south strip of grooved terrain at center of image, offset by nearly its width by transverse fault (image centered at about latitude −15°, longitude 20°; ~1200 km in width; resolution ~3 km/lp); (b) striking differences in morphology and crater density between the darker cratered terrain and the lighter grooved terrain (image centered at 15°, 340°; ~1000 km in width; resolution ~2.5 km/lp); and (c) complex pattern of grooved terrain near the terminator (image centered at about 45°, 300°; ~1000 km in width; resolution 2.5 km/lp).

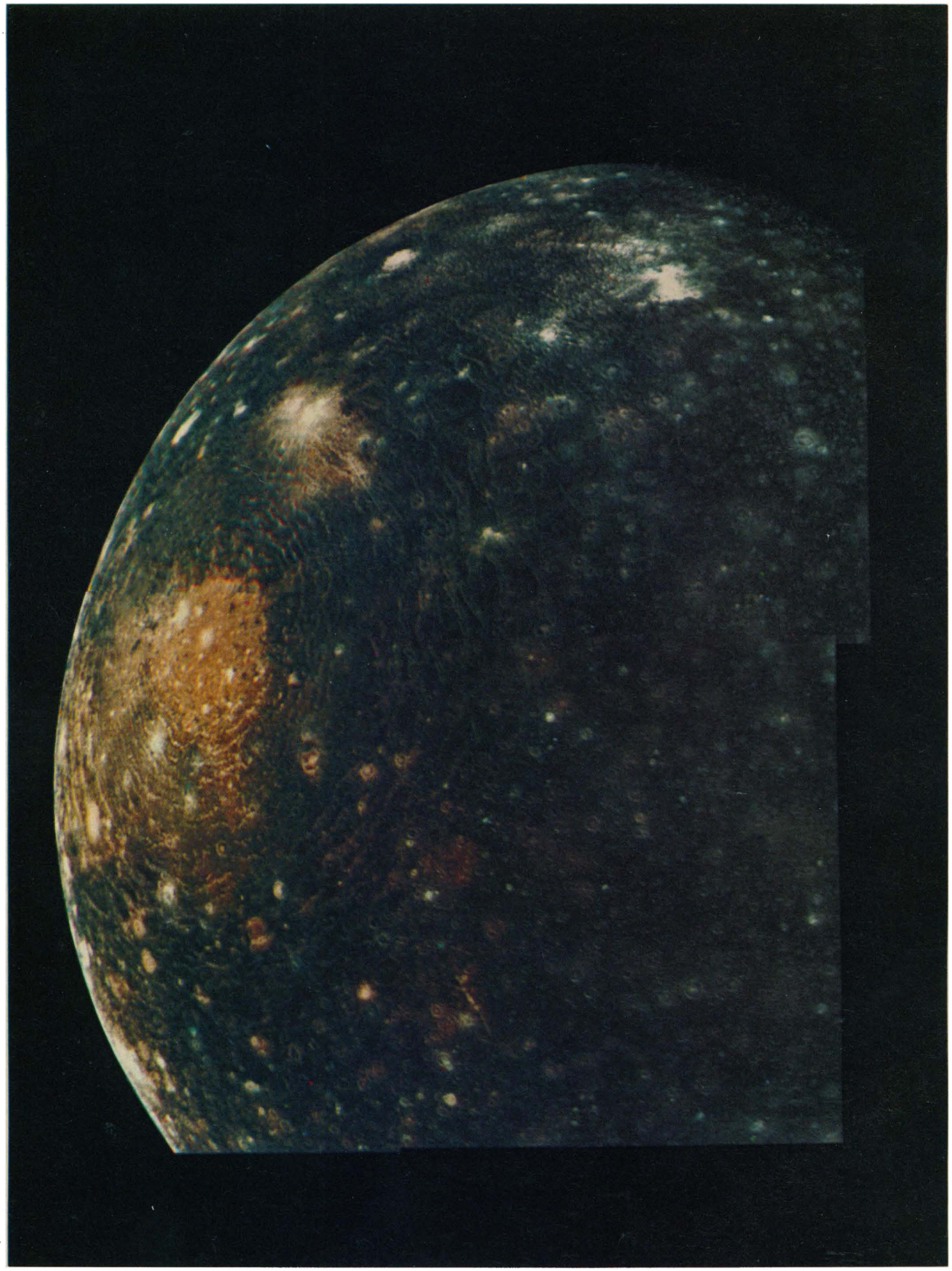

Fig. 22. Computer-generated four-frame color mosaic of Callisto (resolution −7 km/lp). The center of the visible portion of Callisto is near latitude 10°, longitude 0°. The large multi-ring structure is centered at about 10°, 55°.

Voyager 1, several modifications are being made to the Voyager 2 observational sequence in order to obtain color coverage of Jupiter's ring or rings from several positions near the ring plane, improve temporal coverage of dark-side phenomena on Jupiter, and acquire a time-lapse color sequence of volcanic eruptions on the limb of Io.

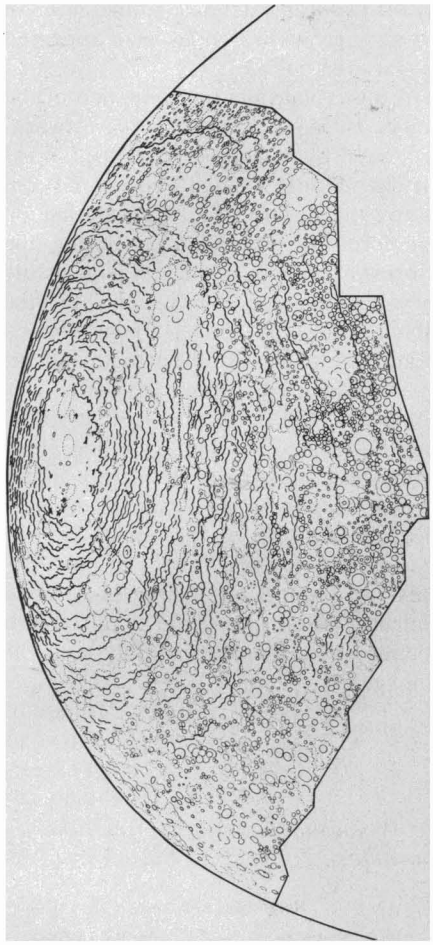

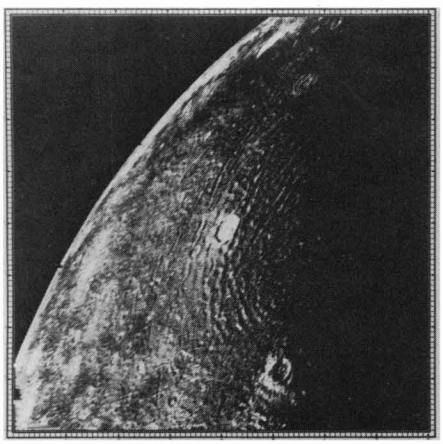

Fig. 23 (top). Sketch map of craters in the region of the large multi-ring structure on Callisto. The rings and large craters are outlined to show the lower density of craters superposed on this feature relative to the average on Callisto. Fig. 24 (bottom). Terminator view of a multi-ring structure on Callisto. This image shows a second multi-ring structure centered on the terminator about latitude 45°, longitude 140°. Smaller than the large ringed structure shown in Fig. 22, the outermost ring seen in this image is about 600 km in radius (resolution −3 km/lp, width ~1200 km).

BRADFORD A. SMITH
Department of Planetary Sciences, University of Arizona, Tucson 85721
LAURENCE A. SODERBLOM
U.S. Geological Survey, Flagstaff, Arizona 86001
TORRENCE V. JOHNSON
Jet Propulsion Laboratory, Pasadena, California 91103
ANDREW P. INGERSOLL
Division of Geological and Planetary Sciences, California Institute of Technology, Pasadena 91125
STEWART A. COLLINS
Jet Propulsion Laboratory
EUGENE M. SHOEMAKER
U.S. Geological Survey, Flagstaff
G. E. HUNT
University College London, London WC 1E 6BT, England
HAROLD MASURSKY
U.S. Geological Survey, Flagstaff
MICHAEL H. CARR
U.S. Geological Survey, Menlo Park, California 94025
MERTON E. DAVIES
Rand Corporation, Santa Monica, California 90406
ALLAN F. COOK II
Smithsonian Astrophysical Observatory, Cambridge, Massachusetts 02138
JOSEPH BOYCE
U.S. Geological Survey, Flagstaff
G. EDWARD DANIELSON
California Institute of Technology
TOBIAS OWEN
Department of Earth and Space Sciences, State University of New York, Stony Brook 11790
CARL SAGAN
Cornell University, Ithaca, New York 14853
RETA F. BEEBE
Department of Astronomy, New Mexico State University, Las Cruces 88003
JOSEPH VEVERKA
Cornell University
ROBERT G. STROM
Lunar and Planetary Laboratory, University of Arizona
JOHN F. MCCAULEY
U.S. Geological Survey, Flagstaff
DAVID MORRISON
Institute for Astronomy, University of Hawaii, Honolulu 96822
GEOFFREY A. BRIGGS
NASA Headquarters, Washington, D.C. 20546
VERNER E. SUOMI
Space Science and Engineering Center, University of Wisconsin, Madison 53706

References and Notes

1. Detailed characteristics of the two Voyager cameras are described elsewhere (*2*). In brief, images are exposed by each camera, through one of eight spectral filters, on the photoconductive surface of a 1-inch selenium-sulfur vidicon. The resulting charge distribution is then scanned by an electron beam, sampled, and digitized to produce an array (800 lines by 800 samples) of eight-bit picture elements. Additional instrumental characteristics are as follows. The narrow-angle camera focal length is 1502.38 mm; field of view, 7.41×10^{-3} radian; focal number, *f*/8.5; and picture element spacing, 9.27 microradians. The spectral filter effective wavelengths (in micrometers) for the narrow-angle camera are ultraviolet, 0.351; violet, 0.413; blue, 0.479; green, 0.564; orange, 0.585; and clear, 0.477. The wide-angle camera focal length is 200.465 mm; field of view, 55.56×10^{-3} radian; focal number, *f*/3.5; and picture element spacing, 69.46 microradians. The spectral filter effective wavelengths (in micrometers) for the wide-angle camera are violet, 0.431; blue, 0.477; methane (1), 0.541; green, 0.572; sodium, 0.589; orange, 0.614; methane (2), 0.619; and clear, 0.507.
2. B. A. Smith *et al.*, *Space Sci. Rev.* **21**, 103 (1977).
3. We use the System III "radio" rotation period of 9 hours, 55 minutes, 29.7 seconds, which is presumed to represent the rotation of the deeper, more viscous regions of Jupiter's atmosphere [see A. C. Riddle and J. W. Warwick, *Icarus* **27**, 457 (1976)].
4. A line pair is two picture element (pixel) spacings in the 800 by 800 array of the Voyager image format.
5. R. J. Terrile and R. F. Beebe, *Science* **204**, 948 (1979).
6. B. M. Peek, *The Planet Jupiter* (Faber & Faber, London, 1958); B. A. Smith and G. E. Hunt, in *Jupiter*, T. Gehrels, Ed. (Univ. of Arizona Press, Tucson, 1976), p. 564.
7. S. L. Hess and H. A. Panofsky, in *Compendium of Meteorology*, T. F. Malone, Ed. (American Meteorological Society, Boston, 1951), p. 391; A. P. Ingersoll and J. N. Cuzzi, *J. Atmos. Sci.* **26**, 981 (1969).
8. R. J. Terrile and J. A. Westphal, *Icarus* **30**, 274 (1977); C. S. L. Keay *et al.*, *Astrophys. J.* **183**, 1063 (1973); R. L. Wildey *et al.*, *J. Geophys. Res.* **70**, 3711 (1965); G. S. Orton and A. P. Ingersoll, in *Jupiter*, T. Gehrels, Ed. (Univ. of Arizona Press, Tucson, 1976), p. 206.
9. T. Gehrels, in *Jupiter*, T. Gehrels, Ed. (Univ. of Arizona Press, Tucson, 1976), p. 531.
10. J. W. Fountain and B. A. Smith, in preparation.
11. R. S. Lindzen, *J. Atmos. Sci.* **31**, 156 (1974).
12. T. Owen, *Icarus* **10**, 473 (1969); ____ and H. P. Mason, *J. Atmos. Sci.* **35**, 101 (1969).
13. R. Hanel *et al.*, *Science* **204**, 972 (1979).
14. A. P. Ingersoll, *ibid.* **182**, 1346 (1973); T. Maxworthy and L. G. Redekopp, *Icarus* **29**, 261 (1976); G. P. Williams, *J. Atmos. Sci.* **35**, 1399 (1978).
15. B. N. Turman, *J. Geophys. Res.* **82**, 2566 (1977); R. D. Hill, *Rev. Geophys. Space Phys.* **17**, 155 (1979).
16. M. H. Acuña and N. F. Ness, *J. Geophys. Res.* **81**, 2917 (1976).
17. E. C. Stone and A. L. Lane, *Science* **204**, 945 (1979).
18. D. Morrison and J. A. Burns, in *Jupiter*, T. Gehrels, Ed. (Univ. of Arizona Press, Tucson, 1976), p. 991.
19. A technique developed by J. Lorre (Image Processing Laboratory, JPL) locates the limb by using a threshold data number (DN) as input. A second technique, written by P. Kupferman (Optical Navigation, JPL), compensates for the vidicon beam bending and locates the limb by finding the inflection point. A third technique, written by M. Davies (Rand Corporation), defines the limb by the inflection point in the DN's and uses only a few points near reseau marks to calibrate the picture measures.
20. G. H. Rieke, *Icarus* **25**, 233 (1975).
21. R. L. Millis, *ibid.* **33**, 319 (1978).
22. J. B. Murray, *ibid.* **25**, 397 (1975); D. B. Nash, *Icarus*, in press; R. B. Minton, *Commun. Lunar Planet. Lab* **10**, 35 (1973).
23. L. A. Soderblom, in *Impact and Explosion Cratering*, D. J. Roddy, R. O. Pepin, R. B. Merrill, Eds. (Pergamon, New York, 1977), p. 629; E. M. Shoemaker, in *ibid.*, p. 617.
24. G. W. Wetherill, in *ibid.*, p. 613.
25. L. A. Morabito, S. P. Synnott, P. N. Kupferman, S. A. Collins, *Science* **204**, 972 (1979).
26. S. J. Peale *et al.*, *ibid.* **203**, 892 (1979).
27. W. Wamstekor, *Commun. Lunar Planet. Lab.* **9**, 171 (1973); F. P. Fanale, T. V. Johnson, D. L. Matson, *Science* **186**, 922 (1974).

28. D. B. Nash and F. P. Fanale, *Icarus* **31**, 40 (1977).
29. I. Kupo *et al.*, *Astrophys. J.* **205**, L51 (1976).
30. A. L. Broadfoot *et al.*, *Science* **204**, 979 (1979).
31. R. L. Nelson and B. W. Hapke, *Icarus* **36**, 304 (1978).
32. C. B. Pilcher, S. T. Ridgway, T. B. McCord, *Science* **178**, 1087 (1972).
33. F. P. Fanale *et al.*, in *Planetary Satellites*, J. A. Burns, Ed. (Univ. of Arizona Press, Tucson, 1977), p. 379.
34. G. J. Consolmagno and J. S. Lewis, in *ibid.*, p. 492.
35. R. T. Reynolds and P. M. Cassen, *Geophys. Res. Lett.* **6**, 121 (1979).
36. T. V. Johnson and T. R. McGetchin, *Icarus* **18**, 612 (1973).
37. L. A. Lebofsky, *Nature (London)* **269**, 785 (1977); J. V. Pollack *et al.*, *Icarus* **36**, 271 (1978).
38. J. F. McCauley, *Phys. Earth Planet Interiors* **15**, 220 (1977).
39. D. Morrison, D. P. Cruikshank, J. A. Burns, in *Planetary Satellites*, J. A. Burns, Ed. (Univ. of Arizona Press, Tucson, 1977), p. 12.
40. P. H. Smith, *Icarus* **35**, 169 (1978).
41. J. D. Anderson, G. W. Null, S. K. Wong, *J. Geophys. Res.* **79**, 3361 (1974).
42. The success of this experiment has in a very real sense resulted directly from the individual contributions of several hundred men and women. Among these are the following: G. Bailey, H. T. Enmark, R. F. Lockhart, L. L. Simmons, and F. E. Vescelus (camera engineering); C. C. Avis, G. W. Garneau, P. L. Jepsen, J. J. Lorre, J. A. Mosher, D. J. Royer, A. A. Schwartz, M. J. Sullivan, G. M. Yagi, and the personnel of JPL's Mission Imaging Operations Group (data processing); R. Batson, P. Bridges, J. Inge, C. Isbell, B. K. Luchitta, G. G. Schaber, and R. Tyner (analysis and cartography); J. L. Anderson, R. P. Laeser, A. L. Lane, M. J. Sander, and C. H. Stembridge (project leadership); R. Gurrola, J. T. Harwood, R. Krauss, V. J. Nelson, L. Pieri, F. Popescu, and JPL's Photolab (supporting efforts); and especially M. L. Brownell, C. J. Hansen, P. N. Kupferman, J. L. Mitchell, and the Voyager Sequence Team for their skilled and tireless efforts to coax such magnificent data from a complicated and sometimes reluctant spacecraft. G. E. Hunt is supported by the Science Research Council, Great Britain. This report presents the results of one phase of research carried out at JPL under NASA contract NAS 7-100. We are grateful for careful reviews of the manuscript by M. Malin, D. Muhleman, J. Pearl, and R. Terrile.

17 April 1979

Discovery of Currently Active Extraterrestrial Volcanism

Abstract. *Two volcanic plumes were discovered on an image of Io taken as part of the Voyager optical navigation effort. This is the first evidence of active volcanism on any body in the solar system other than Earth.*

A photograph of Io (Fig. 1) taken by Voyager 1 revealed the first evidence of currently active volcanism on any solar system object other than Earth. This image was taken at 13:28 Greenwich mean time on 8 March 1979 from a range of 4.5×10^6 km. Io was photographed at this time as part of the Voyager optical navigation effort, a program to determine both the ephemerides of the five inner Jovian satellites and the trajectory of the spacecraft through the acquisition and analysis of satellite and star images.

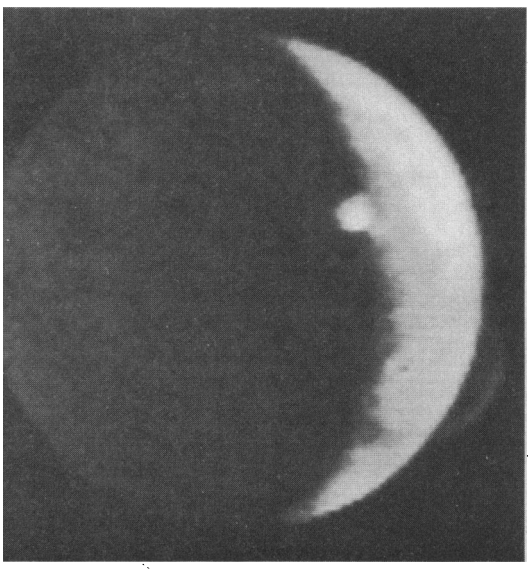

Fig. 1. Narrow-angle image of Io. This 0.96-second exposure was taken through a clear filter by Voyager 1, 3 days after the spacecraft's closest approach to Jupiter. The phase angle is 124°. The image has been digitally enhanced, in contrast and size, to more clearly show the faint cloud above Io's limb. Io's lit crescent is shown as well as its dark hemisphere, which is faintly illuminated by sunlight reflected by Jupiter. Two examples of volcanic plumes are found in this image.

Although not shown in Fig. 1, the original image includes two stars (AGK3-10021 and AGK3-20006). It was the digital processing used to display these faint stars that first revealed a dim cloud (< 10 percent of Io's brightness), which is apparent in the image as a thin crescent above the satellite's eastern limb. It appeared that this crescent might be a second solid body located beyond Io. However, this possibility was ruled out on two bases. First, the diameter of such an object would be sufficient—1000 km or greater—that it should have been previously detected, and second, the spacecraft was about 3° above the orbital plane of the Galilean satellites, so that none of these large bodies could have appeared in line with Io.

A more plausible interpretation of the image is that sunlight is being forward-scattered by a large, well-defined cloud of gas or dust located at least 270 km above the surface of Io. Considering the landforms observed on Io during the closest approach, this cloud is probably of volcanic origin. The cloud is located above, or nearly above, a heart-shaped feature on Io that has been independently identified as a volcanic landform. This feature, at 250° longitude, −30° latitude, can be located on figures 14 and 16 of (*1*), which contains additional examples and a discussion of Io volcanism. Subsequent analysis of this image has revealed that the bright spot at 305°, 10° (just beyond Io's terminator) is a second volcanic plume [see figure 19 in (*1*)] projecting above the dark surface into the sunlight.

L. A. Morabito
S. P. Synnott
P. N. Kupferman
Stewart A. Collins
Jet Propulsion Laboratory, California Institute of Technology, Pasadena 91103

References and Notes

1. B. A. Smith *et al.*, *Science* **204**, 951 (1979).
2. This report presents the results of one phase of research carried out at the Jet Propulsion Laboratory under NASA contract NAS 7-100.

25 April 1979

Infrared Observations of the Jovian System from Voyager 1

Abstract. *The infrared spectroscopy and radiometry investigation has obtained spectra of Jupiter and its satellites between approximately 180 and 2500 cm^{-1} with a spectral resolution of 4.3 cm^{-1}. The Jupiter spectra show clear evidence of H_2, CH_4, C_2H_2, C_2H_6, CH_3D, NH_3, PH_3, H_2O, and GeH_4. A helium concentration of 0.11 ± 0.03 by volume is obtained. Meridional temperature cross sections show considerable structure. At high latitudes, the stratosphere is warmer in the north than in the south. The upper troposphere and lower stratosphere are locally cold over the Great Red Spot. Amalthea is warmer than expected. Considerable thermal structure is observed on Io, including a relatively hot region in the vicinity of a volcanic feature.*

The Voyager infrared spectroscopy and radiometry investigation uses a Michelson interferometer operating in the infrared and a single-channel radiometer sensitive to visible radiation, both of which share a 50-cm Cassegrain telescope. This instrument, designated by the acronym IRIS (*1*), performed well during the Jupiter encounter, with more than 50,000 spectra recorded. Because of a small misalignment that developed during cruise between Earth and Jupiter, satisfactory responsivity of the interferometer is limited to the region be-

0036-8075/79/0601-0972$00.50/0